

# Introduction to parton-shower event generators

Stefan Höche<sup>1</sup>

<sup>1</sup> SLAC National Accelerator Laboratory, Menlo Park, CA 94025, USA

**Abstract:** This lecture discusses the physics implemented by Monte Carlo event generators for hadron colliders. It details the construction of parton showers and the matching of parton showers to fixed-order calculations at higher orders in perturbative QCD. It also discusses approaches to merge calculations for a varying number of jets, the interface to the underlying event and hadronization.

## 1 Introduction

Hadron colliders are discovery machines. The fact that proton beams can be accelerated to higher kinetic energy than electron beams favors hadron colliders over lepton colliders when it comes to setting the record collision energy. But it comes at a cost: Because of the composite nature of the beam particles, the event structure at hadron colliders is significantly more complex than at lepton colliders, and the description of full final states necessitates involved multi-particle calculations. The high-dimensional phase space leaves Monte-Carlo integration as the only viable option. Over the past three decades, this led to the introduction and development of multi-purpose Monte-Carlo event generators for hadron collider physics [1, 2]. This lecture series discusses some basic aspects in the construction of these computer programs.

### 1.1 Stating the problem

The search for new theories of nature which explain the existence of dark matter and dark energy is the focus of interest of high-energy particle physics today. One possible discovery mode is the creation of dark matter candidates at ground-based collider experiments like the Large Hadron Collider (LHC).

However viable a given new physics scenario might be, all potential hadron collider signatures have in common that they will be hidden by overwhelming Standard Model backgrounds. The large phase space at the LHC, for example, typically leads to the creation of  $\mathcal{O}(100) - \mathcal{O}(1000)$  particles. Their momenta can span several orders of magnitude, and they may be subject to intricate kinematical restrictions imposed by the detector geometry. The most pressing problem preventing the accurate prediction of such final states is the non-abelian nature of Quantum Chromodynamics (QCD), which leads to color confinement at long distances. For the complex final states in question, a first-principles approach to this phenomenon is currently out of reach. The two main problems which arise are the description of hadron formation and the evolution of QCD final states from short to long distances. Both can, however, be tackled to a good approximation by Monte-Carlo event generators.

In addition to QCD effects, electroweak interactions will complicate the event structure. Most notably, the emission of soft photons in Bremsstrahlung processes may occur whenever charged particles are

produced in the final state. The computation of such processes will not be discussed in these lectures. The interested reader is referred to the many excellent reviews in the literature [2].

## 1.2 Factorization of the cross section

The production of a high invariant-mass final state, or a reaction with large invariant momentum transfer, can be described using the factorization Ansatz [3, 4, 5]. The inclusive cross section for the production of the final state  $X$  (for example a Drell-Yan lepton pair, or a Higgs boson) in the collision of hadron  $h_1$  and  $h_2$ , is then given by the convolution

$$\sigma_{h_1 h_2 \rightarrow X} = \sum_{a,b \in \{q,g\}} \int dx_a \int dx_b f_a^{h_1}(x_a, \mu_F^2) f_b^{h_2}(x_b, \mu_F^2) \int d\Phi_{ab \rightarrow X} \frac{d\hat{\sigma}_{ab}(\Phi_{ab \rightarrow X}, \mu_F^2)}{d\Phi_{ab \rightarrow X}}. \quad (1.1)$$

The functions  $f_a^h(x, \mu_F^2)$  are the parton distribution functions (PDFs) in collinear factorization. At leading order in perturbative QCD they represent the probability for resolving a parton of flavor  $a$  with momentum fraction  $x$  in the parent hadron  $h$  at the factorization scale  $\mu_F$ .  $d\sigma_{ab}/d\Phi$  denotes the differential cross section for the production of the final state  $X$  from the partonic initial state, and  $d\Phi_{ab \rightarrow X}$  is the corresponding differential final-state phase-space element.

Equation (1.1) determines the total cross section for the production of the final state  $X$ , but it does not specify anything beyond. This means in particular that any number of particles may emerge alongside  $X$  and that  $X$  can assume any kinematical configuration. We therefore call Eq. (1.1) the inclusive cross section for  $X$ -production. Exclusive cross sections can in principle be obtained by restricting the phase space for  $X$ , or by requiring a certain number of additional particles, or both. The approach followed in event generators is different: Starting from Eq. (1.1), an inclusive final state is first produced, which consists only of  $X$ . This configuration is augmented by additional particles in a Markov process, where four-momentum and probability are conserved in the creation of each new particle.<sup>1</sup> Eventually, a high-multiplicity final state emerges which still respects the inclusivity requirement with respect to the production of the original final state of interest. In the following we will identify the relevant Markov processes. One of them is what is called a parton shower.

## 1.3 Collinear factorization and parton showers

The factorization of scattering amplitudes in the collinear limit [6, 7] allows to derive evolution equations like the DGLAP equations [8, 9, 10, 11], which determine the behavior of the PDFs in collinear factorization with changing factorization scale:

$$\mu_F^2 \frac{df_a(x, \mu_F^2)}{d\mu_F^2} = \sum_{b \in \{q,g\}} \int_x^1 \frac{dz}{z} \frac{\alpha_s}{2\pi} \hat{P}_{ba}(z) f_b(x/z, \mu_F^2). \quad (1.2)$$

The functions  $\hat{P}_{ba}(z)$  are the regularized Altarelli-Parisi splitting functions, which describe the collinear splitting of parton  $b$  into parton  $a$ . They are given by

$$\begin{aligned} \hat{P}_{qq}(z) &= C_F \left[ \frac{1+z^2}{(1-z)_+} + \frac{3}{2} \delta(1-z) \right] & \hat{P}_{qg}(z) &= C_F \left[ \frac{1+(1-z)^2}{z} \right] \\ \hat{P}_{gq}(z) &= T_R \left[ z^2 + (1-z)^2 \right] & \hat{P}_{gg}(z) &= 2C_A \left[ \frac{z}{(1-z)_+} + \frac{1-z}{z} + z(1-z) \right] \\ & & &+ \delta(1-z) \left( \frac{11}{6} C_A - \frac{2}{3} n_f T_R \right) \end{aligned} \quad (1.3)$$

Schematically, the DGLAP evolution equation is shown in Fig. 1. It can be interpreted in a straightforward manner: Any parton  $a$ , resolved in the parent hadron at scale  $\mu_F^2$ , may have been produced by the

<sup>1</sup> A slight exception to this rule is the transition from the perturbative to the non-perturbative regime, which will be discussed in Sec. 6.

$$\begin{aligned}
\frac{d}{d \log(t/\mu^2)} \text{---} f_q(x,t) \text{---} q &= \int_x^1 \frac{dz}{z} \frac{\alpha_s}{2\pi} \text{---} P_{qq}(z) \text{---} q + \int_x^1 \frac{dz}{z} \frac{\alpha_s}{2\pi} \text{---} P_{gq}(z) \text{---} q \\
\frac{d}{d \log(t/\mu^2)} \text{---} f_g(x,t) \text{---} g &= \sum_{i=1}^{2n_f} \int_x^1 \frac{dz}{z} \frac{\alpha_s}{2\pi} \text{---} P_{qg}(z) \text{---} g + \int_x^1 \frac{dz}{z} \frac{\alpha_s}{2\pi} \text{---} P_{gg}(z) \text{---} g
\end{aligned}$$

**Figure 1:** Pictorial representation of the DGLAP evolution of PDFs. The white blob represents the incoming hadron.

branching of parton  $b$ , resolved at scale  $\mu_F^2 + d\mu_F^2$ . This is precisely the Markov process we were looking for. The transition from parton  $b$  to parton  $a$  is naturally accompanied by the production of an additional parton, which accounts for momentum and flavor conservation. The additional particle is ignored when the PDF evolution is computed. In a Monte-Carlo event generator, it is accounted for as an additional final-state particle, and the production process is called initial-state radiation.

It is clear that repeated implementation of Eq. (1.2) leads to arbitrarily many parton splittings, and therefore arbitrarily many particles in the final state. The basic idea leading to parton shower Monte Carlo event generators is to use Eq. (1.2) to convert the inclusive prediction for the occurrence of parton  $a$  in the beam hadron  $h$  into an exclusive prediction for parton  $a$  and a certain number of additional particles, which are resolved at smaller and smaller momentum transfer. Two problems remain to be solved.

- The DGLAP equations are derived in the strict collinear limit, i.e. any final-state particles are precisely collinear to the beam particle. If four momentum were conserved, this assumption would imply a vanishing virtuality of the  $t$ -channel propagator, which conflicts with the requirement that  $\mu_F$  be finite.
- The DGLAP equations are fully inclusive, in the sense that parton momenta are integrated over the entire available phase space. Quantum Chromodynamics instead imposes a resolution scale set by  $\Lambda_{\text{QCD}}$ .

The first problem is solved in Monte-Carlo event generators by momentum mapping schemes or “recoil schemes”, which define unambiguously how the kinematics of the process is affected when initial-state radiation occurs. This can be interpreted as a method to assign “spectators”, which may be a single particle or multiple particles, that absorb the “recoil” when a “splitter” particle that was formerly on mass-shell branches into two on-shell particles. It is obvious that if the splitter has zero on-shell mass, this can only be achieved through absorption of kinetic energy from another part of the reaction, the spectator.

The second problem is solved by truncating the evolution at a scale of order  $\Lambda_{\text{QCD}}$ . Due to the fact that parton showers implement four-momentum conservation, this implies a restricted range in the integral over energy fractions in the DGLAP equation, Eq. (1.2). In the following, we discuss the implications of these modifications.

## 1.4 Basic parton-shower kinematics

Consider the splitting process depicted in Fig. 2. All particles are assumed to have zero on-shell mass. We parametrize their momenta in terms of the light-cone momenta  $p_a$  and  $n$ , where  $n$  is a light-like

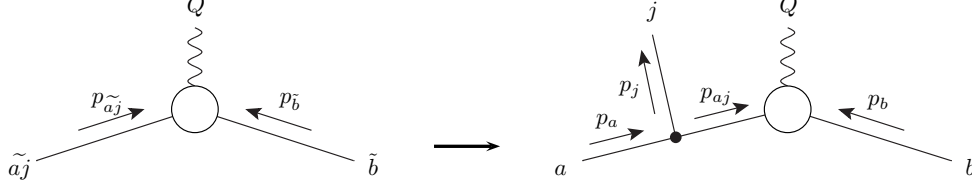


**Figure 2:** Kinematics in the initial-state parton splitting process  $a \rightarrow \{aj\}j$ . The virtuality of parton  $\{aj\}$  entering the hard process is given by  $t$ , while its light-cone momentum fraction with respect to the new initial-state parton is  $z$ . The splitting process has an azimuthal symmetry, which may be broken if the  $t$ -channel parton is a gluon and the hard process has a non-trivial Lorentz structure.

reference vector that satisfies  $np_a \neq 0$ . We can then use the Sudakov decomposition [12]

$$p_{aj}^\mu = \tilde{z} p_a^\mu + \frac{-2p_a p_j + k_\perp^2}{\tilde{z}} \frac{n^\mu}{2np_a} + k_\perp^\mu, \quad p_j^\mu = (1 - \tilde{z}) p_a^\mu + \frac{k_\perp^2}{1 - \tilde{z}} \frac{n^\mu}{2np_a} - k_\perp^\mu. \quad (1.4)$$

In parton shower generators,  $n$  is identified with the spectator momentum, i.e. the momentum of the particle (or set of particles), which recoils against the splitter. If the spectator has zero mass, like in our example,  $2np_a$  can be identified with the invariant mass of the radiating color dipole. We will use this concept extensively in the future. A more precise definition of color dipoles will be given in Sec. 2. For now we work under the assumption that the final state  $X$  does not carry color charge, hence the spectator parton is the opposite-side beam particle. We can then replace  $n$  with  $p_b$ .

Clearly, any recoil scheme must satisfy the condition that the new initial-state momentum after splitting,  $p_a$ , is parallel to the beam direction. We compute it by rescaling:

$$p_a^\mu = \frac{p_a p_b}{p_{a\tilde{j}} p_b} p_{a\tilde{j}}^\mu. \quad (1.5)$$

A peculiarity of initial-state evolution is that the spectator momentum must also remain aligned with the beam axis. In the simplest possible scheme we have  $p_b = p_{\tilde{b}}$ . Since  $p_c$  is not collinear to the beam, the final state  $X$  must absorb all transverse momentum generated in the splitting, but it does not change its invariant mass. This leads to a Lorentz transformation, which acts on all final-state momenta  $p_i$  as [13]

$$p_i^\mu = p_i^\mu - \frac{2p_i(K + \tilde{K})}{(K + \tilde{K})^2} (K + \tilde{K})^\mu + \frac{2p_i \tilde{K}}{\tilde{K}^2} K^\mu, \quad \text{where} \quad K^\mu = p_a^\mu - p_j^\mu + p_b^\mu, \quad \tilde{K}^\mu = p_{a\tilde{j}}^\mu + p_b^\mu \quad (1.6)$$

It is the repeated application of this Lorentz transformation which resums large logarithmic corrections to the transverse momentum of the Higgs boson, for example. The relation between the transverse momentum,  $k_T$ , generated in a single splitting and the corresponding light-cone momentum fraction,  $\tilde{z}$ , is given by

$$k_T^2 = -t(1 - \tilde{z}), \quad \text{where} \quad t = -2p_a p_j. \quad (1.7)$$

Both the transverse momentum and the light-cone momentum fraction are Lorentz invariants, as can be inferred from multiplying Eq. (1.4) by  $n_\mu$ . It follows that the kinematics reconstruction can be achieved in any Lorentz frame. We will now connect the kinematical variables  $t$  and  $\tilde{z}$  to the evolution.

## 1.5 Exclusive evolution equations and Sudakov factors

Partons are bound by confinement into color-neutral hadrons at momentum scales of order  $\Lambda_{\text{QCD}}$ . This implies that both experimentally and theoretically, partons which are closer than about 1 GeV in transverse momentum cannot be separately resolved. This condition introduces a natural cutoff scale for the transverse momentum in Eq. (1.7), which we call the infrared cutoff scale of the parton-shower, or the

parton-shower cutoff,  $t_c$ , for short. Since four-momentum is conserved in each splitting, the cutoff leads to an upper bound on  $\tilde{z}$

$$\tilde{z} = 1 - \frac{k_T^2}{|t|} < 1 - \frac{t_c}{|t_{\max}|} . \quad (1.8)$$

If we identify  $\tilde{z}$  with the energy fraction  $z$  in the DGLAP evolution equations, Eq. (1.2), then the Altarelli-Parisi splitting functions, Eq. (1.3) may be replaced by their unregularized counterparts,  $P_{ba}(z)$ , which are obtained by simply dropping the  $+$ -prescription and the term proportional to  $\delta(1-z)$ .

If we made no further modifications, unitarity would be violated, as we have effectively removed all singularities in the higher-order real-emission contributions to the hard cross section, but also all virtual corrections. This can be remedied by adding an additional term to the DGLAP equations, which reinstates the difference.

$$\frac{df_a(x, t)}{d \log t} = \sum_{b \in \{q, g\}} \int_x^{z_{\max}} \frac{dz}{z} \frac{\alpha_s}{2\pi} P_{ba}(z) f_b(x/z, t) - f_a(x, t) \sum_{b \in \{q, g\}} \int_{z_{\min}}^{z_{\max}} dz \frac{\alpha_s}{2\pi} \frac{1}{2} P_{ab}(z) . \quad (1.9)$$

At the same time we have introduced  $t$  as the evolution variable of our parton shower. We identify this variable with the factorization scale, such that the  $\mu_F^2$  evolution described by Eq. (1.2) turns into a  $t$ -evolution. For now we will leave the precise assignment of  $t$  an open question. It should be identified with a variable which is linear in the virtuality of the intermediate parton, the only dimensionful variable in the splitting process.

Equation (1.9) may be rewritten in a more convenient fashion using the Sudakov form factor

$$\Delta_a(t, t') = \exp \left\{ - \sum_{b \in \{q, g\}} \int_t^{t'} \frac{d\bar{t}}{\bar{t}} \int_{z_{\min}}^{z_{\max}} dz \frac{\alpha_s}{2\pi} \frac{1}{2} P_{ab}(z) \right\} , \quad (1.10)$$

which represents the unconditional survival probability for a parton not to undergo a branching process between the two scales  $t'$  and  $t$ . In terms of  $\Delta$ , Eq. (1.9) becomes the master equation for our parton shower:

$$\frac{d}{d \log t} \log \frac{f_a(x, t)}{\Delta_a(t_c, t)} = \sum_{b \in \{q, g\}} \int_x^{z_{\max}} \frac{dz}{z} \frac{\alpha_s}{2\pi} \hat{P}_{ba}(z) \frac{f_b(x/z, t)}{f_a(x, t)} . \quad (1.11)$$

This equation is solved in one or the other way by any parton-shower Monte-Carlo. All event generators have in common that they use Sudakov factors to account for unresolved splittings and virtual corrections, which are assumed to precisely cancel the real corrections when integrated over phase space. The computation of the Sudakov factor is therefore the principal task for any parton-shower Monte-Carlo event generator. We will discuss the related algorithms in Sec. 3.

Despite all its intricacies, Eq. (1.11) still only leads to an approximate description of fully exclusive final states containing our initial process of interest,  $pp \rightarrow X$ . If detailed experimental measurements are to probe the precise distribution of hard QCD radiation, then we need to improve Eq. (1.11) by replacing the Altarelli-Parisi splitting functions by more precise expressions, at least for the most relevant steps in the evolution. This will be the subject of Sec. 4.

The concept of infrared-safe observables and QCD jets plays a crucial role in this context. Both the initial state and many final states at hadron colliders include hard partons. Initial- and final-state Bremsstrahlung dresses these partons with further radiation, as we have seen above. The new particles are found predominantly in the vicinity of the original ones, leading to clusters of radiation called QCD jets. The jet structure is preserved when hadrons are formed. A cluster of hadronic energy in the experimental measurement can thus be associated with one or more hard initiating partons in the theoretical calculation. For this concept to work an algorithm must be defined that unambiguously relates the two. Crucially, this algorithm must be infrared and collinear safe: if a single parton is replaced by a set of collinear partons sharing its original energy, the jet configuration must not change. Likewise, if a parton of vanishing energy is added to the original event, the identified jet configuration must not change. More details on jet algorithms can be found in [14].

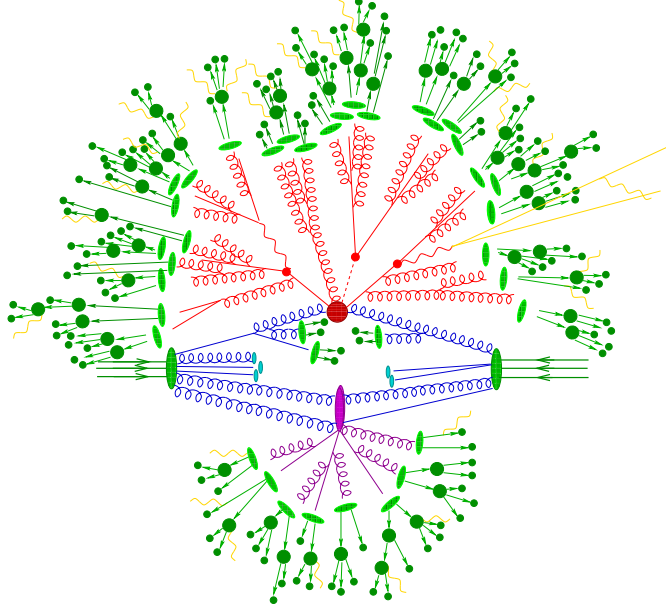


**Figure 3:** Sketch of a hadron-hadron collision as simulated by a Monte-Carlo event generator. The red blob in the center represents the hard collision, surrounded by a tree-like structure representing Bremsstrahlung as simulated by parton showers. The purple blob indicates a secondary hard scattering event. Parton-to-hadron transitions are represented by light green blobs, dark green blobs indicate hadron decays, while yellow lines signal soft photon radiation.

At hadron colliders, multiple scattering and rescattering effects arise, which must be simulated by Monte-Carlo event generators in order to reflect the full complexity of the event structure. This will be discussed in Sec. 5. Eventually we need to convert the full partonic final state into a set of color-neutral hadrons, which is the topic of Sec. 6. The interplay of all these effects makes for the full simulation of hadron-hadron collisions. This is sketched in Fig. 3.

## 2 The hard scattering

Event simulation in parton-shower Monte-Carlo event generators starts with the computation of the hard-scattering cross section at some given order in perturbation theory. Traditionally, this calculation was performed at leading order (LO), but nowadays, with next-to-leading-order (NLO) calculations completely automated, it is often done at NLO. Computing the hard cross section at NLO requires a dedicated matching to the parton shower, which will be discussed in Sec. 4. For now we focus on the evaluation of the differential cross sections and the related phase-space integrals.

The basis for our calculations is the factorization formula, Eq. (1.1). We rewrite it here, in order to simplify the discussions in the following sections. The full initial and final state in a  $2 \rightarrow (n - 2)$  reaction can be identified by a set of  $n$  particles, which is denoted by  $\{\vec{a}\} = \{a_1, \dots, a_n\}$ . Their flavors and momenta are similarly specified as  $\{\vec{f}\} = \{f_1, \dots, f_n\}$  and  $\{\vec{p}\} = \{p_1, \dots, p_n\}$ . The differential cross section at leading order is a sum over all flavor configurations, and it depends only on the parton momenta:

$$d\sigma^{(\text{LO})}(\{\vec{p}\}) = \sum_{\{\vec{f}\}} d\sigma_n^{(\text{B})}(\{\vec{a}\}) , \quad \text{where} \quad d\sigma_n^{(\text{B})}(\{\vec{a}\}) = d\Phi_n(\{\vec{p}\}) B_n(\{\vec{a}\}) . \quad (2.1)$$

Each individual term in the sum consists of the differential phase-space element,  $d\Phi_n$ , the squared matrix

elements,  $|\mathcal{M}_n|^2$ , as well as parton luminosities,  $\mathcal{L}$ , flux ( $F$ ) and symmetry factors ( $S$ )

$$\begin{aligned} \mathcal{B}_n(\{\vec{a}\}) &= \mathcal{L}(\{\vec{a}\}) \mathcal{B}_n(\{\vec{a}\}) , & \mathcal{B}_n(\{\vec{a}\}) &= \frac{1}{F(\{\vec{p}\})} \frac{1}{S(\{\vec{f}\})} |\mathcal{M}_n|^2(\{\vec{a}\}) , \\ d\bar{\Phi}_n(\{\vec{p}\}) &= \frac{dx_1}{x_1} \frac{dx_2}{x_2} d\Phi_n(\{\vec{p}\}) , & \mathcal{L}(\{\vec{a}\}; \mu^2) &= x_1 f_{f_1}(x_1, \mu^2) x_2 f_{f_2}(x_2, \mu^2) . \end{aligned} \quad (2.2)$$

Two challenges arise in the implementation of these formulae:

- The squared matrix elements are tedious to compute if more than two particles are involved in the final state. Problems arise both in the management of the Lorentz structure and of the color structure, as the number of Feynman diagrams grows factorially with the number of external particles.
- The phase-space integrals are hard to evaluate for processes with high particle multiplicity in the final state. As the number of Feynman diagrams grows factorially, so does the number of peaks in the integrand, which are related to particle propagators becoming (close to) on-shell.

Many solutions have been proposed to deal with the above problems. We will review only a few of them here, which are simple and generic and can be implemented regardless of the process in question.

## 2.1 Quantum number management

For each phase-space point, a sum over unobserved external quantum numbers and an averaging over initial states must in principle be performed. This involves in particular the sum over colors and helicities. At the level of squared amplitudes, this sum can be performed analytically, using completeness relations and color algebra. While this leads to structurally simple results and allows analytic insight into the dynamics of the process, it quickly becomes too cumbersome to be carried out at large particle multiplicities, even for powerful computer algorithms, and it is sometimes more useful to compute the sum in a Monte-Carlo fashion. Consider an  $n$ -gluon amplitude: at tree-level, the sum over external states involves  $\mathcal{O}(2^n)$  nonvanishing terms of different helicity. The growth with the number of external states is actually rather mild, and the sum can therefore be computed explicitly. In contrast, the sum over color involves  $\mathcal{O}(8^n)$  terms, which is clearly beyond computational capabilities as soon as  $n$  gets close to eight. It is therefore worth thinking about a method to sample color space efficiently.

A powerful organizing principle for calculations of QCD matrix elements is the expansion in the number of colors,  $N_C$ . It relies on the fact that any octet state of  $SU(3)$  may be represented as a nonet state minus the overcounted singlet, or  $3 \otimes \bar{3} = 8 \oplus 1$ . More specifically <sup>2</sup>

$$T_{ij}^a T_{kl}^a = \delta_{i\bar{l}} \delta_{k\bar{j}} - \frac{1}{N_C} \delta_{ij} \delta_{k\bar{l}} \quad \leftrightarrow \quad \begin{array}{c} \bar{j} \xrightarrow{\quad} k \\ i \xrightarrow{\quad} \bar{l} \end{array} - \frac{1}{N_C} \begin{array}{c} \bar{j} \text{---} \text{---} \text{---} \text{---} k \\ i \text{---} \text{---} \text{---} \text{---} \bar{l} \end{array} . \quad (2.3)$$

This equation relates the octet in color space to two triplet/antitriplet terms. The second term in the expression, which can be interpreted as the overcounted  $U(1)$  gluon, is suppressed by one over the number of colors. In many approximate hard cross section calculations, this term is (partially) dropped in order to ease the computation. This can lead to substantial simplifications, and in some cases is needed to make the calculation possible. Crucially, neglecting this term is also the basis for any standard parton-shower algorithm (although improvements exist, see for example [15]). We will return to this subject in Sec. 3.4.

Consider the computation of an all-gluon amplitude at tree-level. We assume fixed color assignments of the external gluons, i.e. for each external gluon the color index in the adjoint representation of  $SU(3)$  is fixed. We call this amplitude  $\mathcal{M}_n(\{\vec{a}\})$ . It can be factorized into phase-space independent coefficients which are functions of the color structure only, and phase-space dependent partial amplitudes, also called

<sup>2</sup>Note that we normalize the  $SU(3)$  generators as  $T_{ij}^a T_{ji}^b = \delta^{ab}$ . The color-ordered Feynman rules then include an additional factor  $\sqrt{2}$ . Details on this convention are found in [6].

color-ordered amplitudes [16]:

$$\mathcal{M}_n(\{\vec{a}\}) = \sum_{\{\vec{\sigma}\} \in S_{n-1}} \text{Tr} [T^{a_1} T^{a_{\sigma_2}} \dots T^{a_{\sigma_n}}] A_n(1, \sigma_2, \dots, \sigma_n). \quad (2.4)$$

The sum is over all  $(n-1)!$  permutations of the indices  $(2, \dots, n)$ . Each trace corresponds to a particular color structure.  $A_n(1, \sigma_2, \dots, \sigma_n)$  are the partial amplitudes, which depend on the four-momenta  $\{\vec{p}\}$  of the gluons permuted according to  $\{\vec{\sigma}\}$ . The color-ordered amplitudes are much easier to calculate than the full amplitude, as they contain only planar Feynman diagrams.

The decomposition in Eq. (2.4) is not unique. A method better suited to Monte-Carlo treatment is the color-flow decomposition. As the name suggests, it corresponds to identifying the color flow in terms of fundamental 3 and  $\bar{3}$  indices, which then also define the color state of external gluons in  $\mathcal{M}_n$  [17, 18]. The main advantage is that color factors are products of delta functions:

$$\mathcal{M}_n(\{\vec{a}\}) = \sum_{\sigma \in S_{n-1}} \delta_{i_1}^{\bar{j}_{\sigma_2}} \delta_{i_{\sigma_2}}^{\bar{j}_{\sigma_3}} \dots \delta_{i_{\sigma_n}}^{\bar{j}_1} A_n(1, \sigma_2, \dots, \sigma_n). \quad (2.5)$$

Equation (2.5) is straightforwardly implemented in a computer program, since no costly matrix multiplications of complex valued matrices has to be performed, but only integer comparisons. Similar decompositions exist for all tree-level parton amplitudes including any number of quark pairs, gluons and color-singlet objects.

In order to compute the color-summed matrix element squared, we need to square Eq. (2.4) and sum over adjoint color indices assigned to the external gluons. Alternatively, we can square Eq. (2.5) and sum over  $3 \otimes \bar{3}$  indices assigned to the external gluons. However, Eq. (2.5) squared already is a theoretically meaningful result (although not a measurable one). Instead of explicitly summing color flows we may sample them using Monte-Carlo methods. In this case the computational effort per phase space point is much reduced, because a single color configuration leads to fewer partial amplitudes on average than the sum over all, which by definition includes all  $(n-1)!$  permutations<sup>3</sup> [18]. The additional degrees of freedom introduced through sampling are usually easier to deal with than the large numerical effort of computing the summed squared matrix element at every point in phase space.

## 2.2 Automatic matrix element generation

Many techniques have been introduced for the automatic computation of tree-level matrix elements. We will review only one of them, which is particularly suited to the implementation in a computer algorithm, due to its generality and simplicity. External wavefunctions in this method are computed in the Weyl-van der Waerden formalism [21, 22], and full amplitudes are obtained by means of the Berends-Giele recursive relations. A detailed discussion of this and other techniques can be found in reviews of amplitude calculations [6, 23].

Left- and right-handed Weyl spinors are defined by dotted and undotted spinor indices, such that  $\psi_a$  is a covariant (right-handed) and  $\psi^{\dot{a}}$  is a contravariant (left-handed) spinor. Complex conjugation amounts to dotting and undotting indices, according to

$$\psi_{\dot{a}} = (\psi_a)^* , \quad \psi^a = (\psi^{\dot{a}})^* . \quad (2.6)$$

Spinor indices are lowered and raised using the spinor metric, given in terms of the  $\varepsilon$  tensor as

$$\epsilon^{ab} = \epsilon^{\dot{a}\dot{b}} = \epsilon_{ab} = \epsilon_{\dot{a}\dot{b}} = \begin{pmatrix} 0 & 1 \\ -1 & 0 \end{pmatrix} . \quad (2.7)$$

Extensions of the Pauli matrices are defined in terms of the  $2 \times 2$  unit matrix  $\sigma^0 = \text{I}$  and the Pauli matrices  $\vec{\sigma}$  as  $\sigma^{\mu \dot{a}b} = (\sigma^0, \vec{\sigma})$  and  $\sigma_{ab}^{\mu} = (\sigma^0, -\vec{\sigma})$ . Using this definition, an arbitrary real-valued four

---

<sup>3</sup> A third decomposition of the all gluon amplitude exists, which makes the Kleiss-Kuijf relations manifest and requires the evaluation of only  $(n-2)!$  partial amplitudes [19, 20]. However, this does not invalidate our argument, as the factorial growth in the number of partial amplitudes is still present.



vector  $k^\mu$  can be written as a bispinor:

$$k_{\dot{a}b} = \sigma_{\dot{a}b}^\mu k_\mu = \begin{pmatrix} k^+ & k_\perp \\ k_\perp^* & k^- \end{pmatrix}, \quad \text{where} \quad \begin{aligned} k^\pm &= k^0 \pm k^3 \\ k_\perp &= k^1 + ik^2 \end{aligned} . \quad (2.8)$$

For massless vectors,  $\vec{k}_\perp^2 = k^+ k^-$ , and a spinor  $\xi(k)$  can be determined such that  $k_{\dot{a}b} = \xi_{\dot{a}} \xi_b$ :

$$k_{\dot{a}b} = \xi_{\dot{a}}(k) \xi_b(k), \quad \text{where} \quad \xi_a(k) = \begin{pmatrix} \sqrt{k^+} \\ \sqrt{k^-} e^{i\phi_k} \end{pmatrix}, \quad \phi_k = \arg k_\perp . \quad (2.9)$$

Note that this definition is by no means unique, as an arbitrary phase can be added without changing the physics. Equation (2.8) is also ambiguous, because the  $x$ -,  $y$ - and  $z$ -direction along which  $k_\perp$  and  $k^\pm$  are defined can be changed through a rotation of the Pauli matrices. The final result for the squared matrix element must not depend on these choices. This fact can be used in automated computer programs to automatically test the consistency of the calculation.

In order to decompose massive vectors in terms of bispinors they must first be reduced to massless components. Using an auxiliary vector,  $a^\mu$ , we obtain

$$k^\mu = b^\mu - \kappa a^\mu, \quad \text{where} \quad \kappa = \frac{k^2}{2ak} . \quad (2.10)$$

and therefore

$$k^\mu = \frac{1}{2} \sigma_{\dot{a}b}^\mu b^{\dot{a}b} - \frac{\kappa}{2} \sigma_{\dot{a}b}^\mu a^{\dot{a}b} . \quad (2.11)$$

We introduce the standard shorthand notation which denotes the spinor  $\xi_a(k_i)$  as  $|k_i\rangle$  or  $|k_i^+\rangle$  and the corresponding spinor  $\xi^{\dot{a}}(k_i)$  as  $|k_i]$  or  $|k_i^-\rangle$ . The inner product in spinor space is then given by

$$\langle \xi \eta \rangle = \langle \xi^+ | \eta^+ \rangle = \xi_a \eta^a, \quad [\xi \eta] = \langle \xi^- | \eta^- \rangle = \xi_{\dot{a}} \eta^{\dot{a}}, \quad (2.12)$$

Due to the spinor metric  $\epsilon$ , the inner product is antisymmetric in its arguments and the Schouten identity holds. Equation (2.6) implies  $[\xi \eta] = \langle \xi \eta \rangle^*$ . The invariant mass of a pair of massless particles described by the four vectors  $k_i$  and  $k_j$  is obtained in terms of spinor products as  $2k_i k_j = \langle i^+ | \sigma^\mu | i^+ \rangle \langle j^+ | \sigma_\mu | j^+ \rangle / 2 = \langle ij \rangle [ji]$ . Hence, up to a phase, spinor products are square roots of Lorentz invariants.

To compute full matrix elements we need explicit Dirac spinors and polarization vectors for external states. They can easily be derived in the Weyl-van der Waerden formalism. Dirac spinors are represented in terms of Weyl spinors as

$$\Psi = \begin{pmatrix} \phi^{\dot{a}} \\ \psi_a \end{pmatrix} . \quad (2.13)$$

The corresponding Dirac matrices read

$$\gamma^\mu = \begin{pmatrix} 0 & \sigma^{\mu \dot{a}b} \\ \sigma_{\dot{a}b}^\mu & 0 \end{pmatrix}, \quad \gamma^5 = i\gamma^0 \gamma^1 \gamma^2 \gamma^3 = \begin{pmatrix} -\sigma^0 & 0 \\ 0 & \sigma^0 \end{pmatrix} . \quad (2.14)$$

Covariant and contravariant spinors  $\psi_a$  and  $\phi^{\dot{a}}$  can be singled out using the projectors  $P_\pm = (1 \pm \gamma^5)/2$ . A complete set of Eigenspinors of the Dirac equation can be computed in terms of the variables  $\bar{p} = \text{sgn}(p_0) |\vec{p}|$  and  $\hat{p} = (\vec{p}, \bar{p})$ , as [24]

$$\begin{aligned} u_+(p, m) &= \frac{1}{\sqrt{2\bar{p}}} \begin{pmatrix} \sqrt{p_0 - \bar{p}} \chi_+(\hat{p}) \\ \sqrt{p_0 + \bar{p}} \chi_+(\hat{p}) \end{pmatrix}, & v_-(p, m) &= \frac{1}{\sqrt{2\bar{p}}} \begin{pmatrix} -\sqrt{p_0 - \bar{p}} \chi_+(\hat{p}) \\ \sqrt{p_0 + \bar{p}} \chi_+(\hat{p}) \end{pmatrix}, \\ u_-(p, m) &= \frac{1}{\sqrt{2\bar{p}}} \begin{pmatrix} \sqrt{p_0 + \bar{p}} \chi_-(\hat{p}) \\ \sqrt{p_0 - \bar{p}} \chi_-(\hat{p}) \end{pmatrix}, & v_+(p, m) &= \frac{1}{\sqrt{2\bar{p}}} \begin{pmatrix} \sqrt{p_0 + \bar{p}} \chi_-(\hat{p}) \\ -\sqrt{p_0 - \bar{p}} \chi_-(\hat{p}) \end{pmatrix}. \end{aligned} \quad (2.15)$$

The Weyl spinors  $\chi_\pm(p)$  are given by  $\chi_+(p) = \xi_a(p)$  and  $\chi_-(p) = \xi^{\dot{a}}(p)$ . The above definition has the apparent advantage, that massless Dirac spinors have two nonzero components only. This fact, together with the definition of the Dirac matrices, Eq. (2.14), greatly simplifies computations in massless theories.

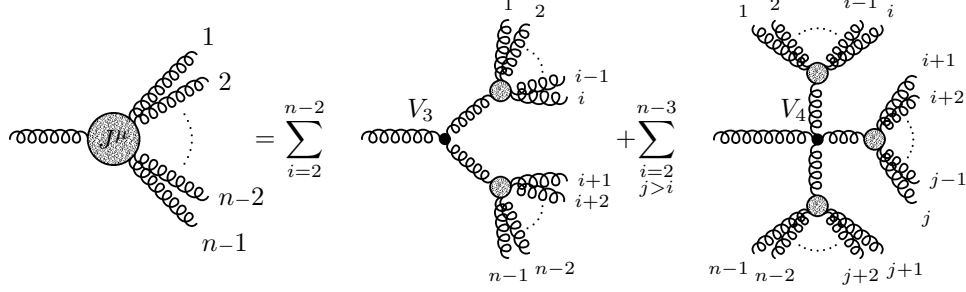


**Figure 4:** Pictorial representation of the Berends-Giele recursion relations, Eq. (2.18).

Polarization vectors for massless external vector bosons can be constructed as

$$\varepsilon_{\pm}^{\mu}(p, k) = \pm \frac{\langle k^{\mp} | \gamma^{\mu} | p^{\mp} \rangle}{\sqrt{2} \langle k^{\mp} | p^{\pm} \rangle} . \quad (2.16)$$

In this context,  $k$  is an arbitrary light-like auxiliary vector, which satisfies  $pk \neq 0$ . This definition leads to the polarization sum of a light-like axial gauge [6, 23]. For massive vector bosons the wave function must satisfy Proca's equation, and we obtain one additional polarization:

$$\varepsilon_{\pm}^{\mu}(p, k) = \pm \frac{\langle k^{\mp} | \gamma^{\mu} | b^{\mp} \rangle}{\sqrt{2} \langle k^{\mp} | b^{\pm} \rangle} , \quad \varepsilon_0^{\mu}(p, k) = \frac{1}{m} ( \langle b^{-} | \gamma^{\mu} | b^{-} \rangle - \kappa \langle k^{-} | \gamma^{\mu} | k^{-} \rangle ) , \quad (2.17)$$

where  $b = p - \kappa k$  and  $\kappa = p^2/2pk$ . Again,  $k$  is an arbitrary light-like gauge vector.

Equations (2.15), (2.16) and (2.17) are sufficient to construct all relevant eigenstates of the external particles in the Standard Model and a wide range of theories beyond it. We will now explain how the full matrix element is efficiently computed using this information.

Berends and Giele introduced an efficient algorithm [25] which generates the color-ordered  $n - 1$ -point gluon off-shell current,  $J^{\mu}$ , defined as the sum of all color-ordered all-gluon Feynman diagrams with  $n - 1$  external legs and a single off-shell leg with polarization  $\mu$ . The recursion relation defining this current reads

$$J^{\mu}(1, 2, \dots, n-1) = \frac{-i}{P_{1,n-1}^2} \left\{ \sum_{k=1}^{n-2} V_3^{\mu\nu\rho}(P_{1,k}, P_{k+1,n-1}) J_{\nu}(1, \dots, k) J_{\rho}(k+1, \dots, n-1) \right. \\ \left. + \sum_{j=1}^{n-3} \sum_{k=j+1}^{n-2} V_4^{\mu\nu\rho\sigma} J_{\nu}(1, \dots, j) J_{\rho}(j+1, \dots, k) J_{\sigma}(k+1, \dots, n-1) \right\} , \quad (2.18)$$

where the momentum sum  $P_{i,j}$  is defined as  $P_{i,j} = \sum_{k=i}^{j-1} p_k$ , and where  $V_3^{\mu\nu\rho}(P_{1,k}, P_{k+1,n-1})$  and  $V_4^{\mu\nu\rho\sigma}$  are the color-ordered three and four-gluon vertices [6]:

$$V_3^{\mu\nu\rho}(P, Q) = i \frac{g_s}{\sqrt{2}} \left( g^{\nu\rho}(P - Q)^{\mu} + 2g^{\rho\mu}Q^{\nu} - 2g^{\mu\nu}P^{\rho} \right) , \\ V_4^{\mu\nu\rho\sigma} = i \frac{g_s^2}{2} \left( 2g^{\mu\rho}g^{\nu\sigma} - g^{\mu\nu}g^{\rho\sigma} - g^{\mu\sigma}g^{\nu\rho} \right) . \quad (2.19)$$

The algorithm is schematically depicted in Fig. 4. The full  $n$ -gluon amplitude is obtained by amputating the off-shell propagator and contracting the remaining quantity with the polarization of gluon  $n$ :

$$A_n(1, \dots, n) = \varepsilon_n^{\mu} \frac{P_{1,n-1}^2}{i} J_{\mu}(1, \dots, n-1) . \quad (2.20)$$

Similar recursions exist for the off-shell quark currents [25], and they can be defined for any gauge theory. Berends-Giele type recursion relations can straightforwardly be implemented into computer programs

and are therefore particularly suited for numerical calculations. They are not limited to color-ordered amplitudes, but can be extended to include color information, which makes the full result equivalent to the Dyson-Schwinger approach used in [17, 26].

The power of recursion relations lies in the fact that for each individual phase-space point, each off-shell current in the calculation must be computed exactly once. It can be reused as a numerical value whenever the computation of Eq. (2.18) necessitates it. This is obviously true not only for a single helicity or color configuration. Currents with a certain assignment of external-particle quantum numbers can be reused no matter what the final amplitude is that needs to be computed. Therefore, the Berends-Giele recursion is a maximally efficient common subexpression elimination for brute force tree-level calculations.

## 2.3 Efficient phase space integration

Generic methods to deal with the problem of high-dimensional phase-space integrals were proposed long ago [27]. The crucial observation is that the integral factorizes into components, which are associated with  $2 \rightarrow 2$  scattering processes,  $1 \rightarrow 2$  decay processes, and  $2 \rightarrow 1$  annihilation processes. The knowledge of propagators and vertices in Feynman diagrams then permits the construction of a Monte-Carlo integrator which precisely maps onto the peak structure of a certain diagram squared. However, each diagram can lead to a different integrator. The multi-channel method is used to combine those and find the optimal balance, such that the full matrix element squared is integrated with maximum efficiency [28].

The differential final-state phase space element for  $2 \rightarrow (n - 2)$  scattering is

$$d\Phi_n(\{\vec{p}\}) = \left[ \prod_{i=3}^n \frac{d^4 p_i}{(2\pi)^3} \delta(p_i^2 - m_i^2) \Theta(E_i) \right] (2\pi)^4 \delta^{(4)} \left( p_1 + p_2 - \sum_{i=3}^n p_i \right), \quad (2.21)$$

where  $m_i$  are the on-shell masses of outgoing particles. Equation (2.21) factorizes as [29]

$$d\Phi_n(p_1, p_2; p_3, \dots, p_n) = d\Phi_{n-m+1}(p_1, p_2; p_3, \dots, p_{n-m}, P) \frac{dP^2}{2\pi} d\Phi_m(P; p_{n-m+1}, \dots, p_n), \quad (2.22)$$

where  $P$  denotes a virtual intermediate particle. Even though this particle has no direct physical interpretation, it may be associated with an  $s$ -channel propagator formed by the set of external states  $\{p_{n-m+1}, \dots, p_n\}$ . If a corresponding propagator exists in any Feynman diagram, the peak structure of this diagram squared can efficiently be mapped out by distributing Monte-Carlo points according to the shape of the propagator squared. This technique is also very efficient for the full matrix element, where the diagram containing the propagator interferes with other diagrams.

Equation (2.22) allows one to decompose the complete phase space into only three elementary building blocks that are given by

$$\begin{aligned} d\Phi_2(p_a, p_b; p_i, p_j) &= \frac{\lambda(s_{ab}, s_i, s_j)}{16\pi^2 2 s_{ab}} d\cos\theta_i d\phi_i, \\ d\Phi_2(p_{ij}; p_i, p_j) &= \frac{\lambda(s_{ij}, s_i, s_j)}{16\pi^2 2 s_{ij}} d\cos\theta_i d\phi_i, \\ d\Phi_1(p_a, p_b; p_i) &= (2\pi)^4 d^4 p_i \delta^{(4)}(p_a + p_b - p_i). \end{aligned} \quad (2.23)$$

We have introduced the Källén function

$$\lambda(s_a, s_b, s_c) = \sqrt{(s_a - s_b - s_c)^2 - 4s_b s_c}. \quad (2.24)$$

Equation (2.23) may be interpreted as elementary  $t$ - and  $s$ -channel “vertices”, while the integral  $dP^2/2\pi$  in Eq. (2.22) corresponds to a “propagator”. This makes the correspondence to tree-level matrix elements manifest. Note that  $d\Phi_2(p_a, p_b; p_i, p_j)$  and  $d\Phi_2(p_{ij}; p_i, p_j)$  are formally identical, since they represent a solid angle integration. However, in practice one chooses different sampling strategies [27] in order to reflect the peak structure of the integrand. The  $s$ -channel annihilation vertex  $d\Phi_1(p_a, p_b; p_i)$  is needed only for bookkeeping. It corresponds to overall momentum conservation and the associated overall weight factor  $(2\pi)^4$ .

Let us investigate the situation where multiple diagrams contribute to a given process, like for example  $gg \rightarrow gg$  scattering. In this case we have three different production channels, and therefore three different integrators, called integration channels. They are  $d\Phi_2(p_1, p_2; p_3, p_4)$ ,  $d\Phi_2(p_1, p_2; p_4, p_3)$  and  $d\Phi_2(p_{12}; p_3, p_4)$ . The task is to find the optimal balance between them. The azimuthal angle integration can be carried out trivially. We can then map the situation onto a single-dimensional integral of a function  $f(x)$  with unknown peak structure, and three “guesstimates” with known integrals, which we call  $g_1(x) \dots g_3(x)$ . We assume that  $f(x)$  is a linear combination of the  $g_i(x)$ . Therefore the primitive of  $f(x)$ ,  $F(x)$ , is also a linear combination of the (known) primitives  $G_i(x) = \int dx g_i(x)$ :

$$f(x) \approx g(x) = \sum_i \alpha_i g_i(x) . \quad (2.25)$$

The set of numbers  $\alpha_i$ , which must be normalized as  $\sum_i \alpha_i = 1$ , is called the a-priori weights of the multi-channel integrator. The task is to adjust these weights automatically, such that the variance of the Monte-Carlo integral is minimized. This procedure is a variant of importance sampling. For it to work it is vital that the Monte-Carlo integral is independent of the integration variable while its variance is not:

$$\begin{aligned} I[f] &= \langle f(x) \rangle_x = \int dx f(x) = \int dG(x) \frac{f(x)}{g(x)} = \langle w(x) \rangle_{G(x)} = I_g[f] , \quad \text{where} \quad w(x) = \frac{f(x)}{g(x)} \\ V[f] &= \langle f^2(x) \rangle_x = \int dx f^2(x) \neq \int dG(x) \left( \frac{f(x)}{g(x)} \right)^2 = \langle w^2(x) \rangle_{G(x)} = V_g[f] \end{aligned} \quad (2.26)$$

The extremum of the variance  $V_g[f]$  is obtained when  $V_{g,i}[f] = V_g[f]$  for all  $i$ , where

$$V_{g,i}[f] = -\frac{\partial}{\partial \alpha_i} V_g[f] = \left\langle \frac{g_i(x)}{g(x)} w^2(x) \right\rangle_{G(x)} . \quad (2.27)$$

This means that all integration channels should contribute equally to the variance. By setting  $\alpha_i \rightarrow \alpha_i \sqrt{V_{g,i}[f]}$  after a certain number of points in the integration, we obtain the best possible approximation of this situation. This example can be extended trivially to the case where  $x$  is a multi-dimensional random variable.

The multi-channel integrator described above can be further refined by using adaptive stratified sampling techniques like Vegas [30]. The factorization of each integration channel into basic building blocks allows for the independent optimization of the grid for each propagator and each vertex. Challenging situations like non-factorizable integrands can be imagined and have been investigated in great detail [31, 32]. However, in practice the combination of factorization, multi-channel integration and adaptive stratified sampling performs reasonably well in most cases.

## 2.4 Next-to-leading order calculations

With the advent of general procedures for the treatment of infrared singularities in QCD [33, 13, 34], existing tree-level matrix element generators became tools to organize ever-more complicated NLO calculations [35, 36]. Crucially, their combination with modern Monte-Carlo event generators enables an automatic matching to the approximate higher-order corrections implemented by parton showers, and it allows one to generate particle-level events at high theoretical accuracy [37, 38, 39]. A full review of modern techniques for NLO QCD calculations is beyond the scope of these lectures. In the following we will focus only on the key components needed at the interface between NLO calculations and parton shower simulations.

Cross sections calculated at NLO accuracy consist of four parts: The Born contribution, the virtual and the real corrections, and the collinear mass factorization counterterms. A genuine obstacle in the calculation is the appearance of ultraviolet and infrared divergences. Ultraviolet terms are dealt with in a rather straightforward manner: Loop amplitudes are regularized in dimensional regularization, and the theory is renormalized by adding counterterms. Infrared divergences are more complicated to handle, as cancellations between the virtual and the real corrections, which are guaranteed by the Bloch-Nordsieck [40]

and Kinoshita-Lee-Nauenberg [41, 42] theorems, occur only after integration over the final-state phase space.

We start by discussing the real-emission contribution. In full analogy to Eqs. (2.1) and (2.2) we write the differential cross section as a sum, depending on parton configurations  $\{a_1, \dots, a_{n+1}\}$ . The Born-level matrix elements  $\mathcal{B}_n$  are replaced by the real-emission matrix elements  $\mathcal{B}_{n+1}$ , and the Born-level phase space  $d\Phi_n$  is replaced by the real-emission phase-space  $d\Phi_{n+1}$ . We introduce a notation for mapping from real-emission parton configurations to Born-level configurations:

$$b_{ij,k}(\{\vec{a}\}) = \left\{ \begin{array}{l} \{\vec{f}\} \setminus \{f_i, f_j\} \cup \{f_{i\bar{j}}\} \\ \{\vec{p}\} \rightarrow \{\vec{p}\} \end{array} \right. . \quad (2.28)$$

The map  $b_{ij,k}(\{\vec{a}\})$  combines partons  $a_i$  and  $a_j$  into a common “mother” parton  $a_{i\bar{j}}$ , in the presence of the spectator  $a_k$  by defining a new flavor  $f_{i\bar{j}}$  and by redefining the particle momenta. This is the exact inverse to the splitting process discussed in Sec. 1.3.

When two partons become collinear, the real-emission matrix element squared factorizes as

$$|\mathcal{M}_{n+1}|^2(\{\vec{a}\}) \xrightarrow{ij \text{ collinear}} \frac{8\pi\alpha_s \mu^{2\varepsilon}}{2p_i p_j} \mathcal{M}_n(b_{ij,\bullet}(\{\vec{a}\})) \otimes \tilde{P}_{i\bar{j}}(z, \varepsilon) \otimes \mathcal{M}_n^*(b_{ij,\bullet}(\{\vec{a}\})) , \quad (2.29)$$

where the  $\otimes$  indicates spin correlations between the Born matrix elements and the spin-dependent Altarelli-Parisi splitting functions,  $\tilde{P}_{ij}(z)$ . In the strict collinear limit, the map does not depend on the spectator parton (cf. Sec. 1.3), which is denoted by the open index marked as  $\bullet$ .

If a single gluon becomes soft, the real-emission matrix element squared behaves as

$$|\mathcal{M}_{n+1}|^2(\{\vec{a}\}) \xrightarrow{j \text{ soft}} -8\pi\alpha_s \mu^{2\varepsilon} \sum_{k>i} \mathcal{M}_n(b_{ij,k}(\{\vec{a}\})) \otimes \mathbf{T}_i \mathbf{T}_k \frac{p_i p_k}{(p_i p_j)(p_j p_k)} \otimes \mathcal{M}_n^*(b_{kj,i}(\{\vec{a}\})) , \quad (2.30)$$

where  $\mathbf{T}_i$  and  $\mathbf{T}_k$  are the color charge operators of the external partons [43].

The collinear and soft singularities can be treated individually, after the final-state phase space has been separated into sectors where only one divergent term contributes [33, 44]. Alternatively, the collinear and soft factorization can be rewritten as a dipole factorization, using splitting functions which capture the singularity structure in both limits, after partial fractioning the soft eikonals [13, 34]. This scheme is called the Catani-Seymour (CS) dipole subtraction method. It allows one to fully regularize the real-emission contribution by adding a set of local counterterms,  $S_{n+1}^{ij,k}(\{\vec{a}\})$ , which are called the dipole subtraction terms. They are defined as

$$S_{n+1}^{ij,k}(\{\vec{a}\}) = -\frac{1}{F(\{\vec{p}\})} \frac{1}{S(\{\vec{f}\})} \frac{8\pi\alpha_s \mu^{2\varepsilon}}{2p_i p_j} \mathcal{M}_n(b_{ij,k}(\{\vec{a}\})) \otimes \frac{\mathbf{T}_{ij} \mathbf{T}_k}{\mathbf{T}_{ij}^2} V_{ij,k}(a_i, a_j, a_k) \otimes \mathcal{M}_n^*(b_{kj,i}(\{\vec{a}\})) , \quad (2.31)$$

Using these terms one can compute arbitrary infrared- and collinear-safe observables, in particular jet observables. This will become important in Sec. 4. We will denote such an observable by  $O$ . Calculating the expectation value of this observable,  $\langle O \rangle$ , is equivalent to an experimental measurement. At NLO QCD we obtain

$$\begin{aligned} \langle O \rangle^{(\text{NLO})} &= \sum_{\{\vec{f}\}} \int d\bar{\Phi}_n(\{\vec{p}\}) \left( \mathcal{B}_n(\{\vec{a}\}) + \tilde{V}_n(\{\vec{a}\}) + \sum_{\{\vec{i}, \vec{k}\}} \mathcal{I}_n^{\vec{i}, \vec{k}}(\{\vec{a}\}) \right) O(\{\vec{p}\}) \\ &\quad + \sum_{\{\vec{f}\}} \int d\bar{\Phi}_{n+1}(\{\vec{p}\}) \left( \mathcal{B}_{n+1}(\{\vec{a}\}) O(\{\vec{p}\}) - \sum_{\{ij,k\}} S_{n+1}^{ij,k}(\{\vec{a}\}) O(b_{ij,k}(\{\vec{p}\})) \right), \end{aligned} \quad (2.32)$$

where, in analogy to Eq. (2.2),  $S^{ij,k} = \mathcal{L} S^{ij,k}$ . The integrated subtraction terms  $\mathcal{I}_n^{\vec{i}, \vec{k}}$  are determined by the analytically integrated insertion operators  $V_{ij,k}(a_i, a_j, a_k)$ , multiplied by Born matrix elements, similar to Eq. (2.31) [13, 34].  $\tilde{V}(\{\vec{a}\})$  represents the virtual corrections after ultraviolet renormalization,

which also include the collinear mass-factorization counterterms. Note that the cancellation of  $I_n^{\tilde{ij},\tilde{k}}$  and  $\sum_{\{ij,k\}} S_{n+1}^{ij,k}(\{\vec{a}\})$ , integrated over the one-parton emission subspace, must be guaranteed locally in the phase-space of the Born process. This is ensured by the observable dependence  $O(b_{ij,k}(\{\vec{p}\}))$  in the last term.

The integrated subtraction terms contain poles in the dimensional regularization parameter  $\varepsilon$ , which cancel the poles in the virtual corrections, such that the first and second sum in Eq. (2.32) are separately infrared finite. This is crucial as the phase-space integrals to be evaluated have a different number of dimensions. Equation (2.32) therefore permits computation of any process at NLO in an automated fashion using the integration techniques of Sec. 2.3. The computation of the real-emission differential cross sections and the corresponding dipole subtraction terms can be fully automated, in the same manner as any tree-level matrix element calculation [45, 46, 47, 48]. The same is true for the integrated subtraction terms. The only missing ingredients to a full NLO calculation are the virtual corrections  $\hat{V}(\{\vec{a}\})$ . They are typically provided to the Monte-Carlo event generator by specialized programs [35, 36], and we will not detail their computation here.

### 3 The parton shower

Parton showers approximate higher-order real-emission corrections to the hard scattering by simulating the branching of a single external parton into two partons. They locally conserve flavor and four momentum, and they respect unitarity, which simply means that a parton may either split into two partons, or it may not. These few very basic requirements are in principle enough to define a parton shower. Many choices can however be made in its precise implementation, and the quality of parton-shower predictions often depends significantly on these choices. A prime example is the selection of an evolution variable representing angular ordering, which itself is a consequence of color coherence. In parton showers using Altarelli-Parisi splitting functions, this choice (or an explicit angular-veto requirement) is needed in order to recover the correct soft anomalous dimension in the evolution. However, angular ordering is not the only way in which color coherence can be ensured. This section will first introduce the basics of parton shower algorithms, including a Monte-Carlo technique known as the veto algorithm, while the choices for evolution variables and evolution kernels as well as their implications are discussed later.

We start with the next-to-leading order dipole subtraction terms, Eq. (2.31). They can be classified according to their Born flavor and momentum configuration, plus an additional flavor and momentum generated by the  $1 \rightarrow 2$  branching process that will be interpreted as a basic parton shower step. This situation is sketched in Fig. 2. We first introduce a notation for mapping from Born parton configurations to real-emission configurations, which is the inverse of Eq. (3.1):

$$r_{\tilde{ij},\tilde{k}}(f_i, \Phi_{+1}^{ij,k}; \{\vec{a}\}) = \left\{ \begin{array}{l} \{\vec{f}\} \setminus \{f_{\tilde{ij}}\} \cup \{f_i, f_j\} \\ \{\vec{p}\} \rightarrow \{\vec{p}\} \end{array} \right. . \quad (3.1)$$

Note that while  $b_{ij,k}(\{\vec{a}\})$  is unambiguously defined by the real-emission parton configuration  $\{\vec{a}\}$ , its inverse,  $r_{\tilde{ij},\tilde{k}}(\{\vec{a}\})$  depends on additional radiative variables  $\Phi_{+1}^{ij,k}$  and a newly-selected flavor. It is the task of the parton-shower algorithm to select these four variables using Monte-Carlo methods.

Crucially, the  $n+1$ -particle phase space factorizes (cf. Sec. 2.3), such that the computation of the next-to-leading order dipole subtraction terms can be reorganized as

$$\sum_{\{\vec{f}\}} d\bar{\Phi}_{n+1} S_{n+1}^{ij,k}(\{\vec{a}\}) \rightarrow \sum_{\{\vec{f}\}} d\bar{\Phi}_n \left[ \sum_{\{\tilde{ij},\tilde{k}\} \in \{\vec{f}\}} \sum_{f_i} d\Phi_{+1}^{ij,k} S_{n+1}^{ij,k}(r_{\tilde{ij},\tilde{k}}(f_i, \Phi_{+1}^{ij,k}; \{\vec{a}\})) \right]. \quad (3.2)$$

Note that the sum over parton configurations is for  $n+1$ -particle configurations on the left-hand side and  $n$ -particle configurations on the right-hand side. The one-particle emission phase-space can be parametrized in terms of three variables, which we will call the evolution variable,  $t$ , the splitting variable,  $z$ , and an azimuthal angle,  $\phi$  (cf. Sec. 1.3):

$$d\Phi_{+1}^{ij,k} = \frac{1}{16\pi^2} dt dz \frac{d\phi}{2\pi} J(t, z, \phi). \quad (3.3)$$

Among these variables, only the evolution variable is dimensionful.  $J(t, z, \phi)$  denotes the Jacobian factor associated with the variable transformation. Next we factor out the Born differential cross section:

$$d\sigma_n^{(B)}(\{\vec{a}\}) = \sum_{\{\tilde{ij}, \tilde{k}\} \in \{\vec{f}\}} \sum_{f_i} d\Phi_{+1}^{ij,k} \frac{S_{n+1}^{ij,k}(r_{\tilde{ij}, \tilde{k}}(f_i, \Phi_{+1}^{ij,k}; \{\vec{a}\}))}{B_n(\{\vec{a}\})}. \quad (3.4)$$

Due to the factorization properties of the real-emission matrix element, Eq. (3.4) is an approximation of real-emission corrections to the leading-order process with configuration  $\{\vec{a}\}$ . It is local in both phase space and flavor space. We call each term in the sum a dipole, for reasons which will become apparent later.

### 3.1 Branching probabilities

At this point it is useful to associate the abstract expression, Eq. (3.4) with a concrete implementation. Taking the collinear limit, and averaging over helicities, we obtain

$$d\sigma_n^{(B)}(\{\vec{a}\}) = \sum_{\{\tilde{ij}, \tilde{k}\} \in \{\vec{f}\}} \sum_{f_i} \frac{S(\{\vec{f}\})}{S(r_{\tilde{ij}, \tilde{k}}(f_i; \{\vec{f}\}))} dt dz \frac{1}{2 p_i p_j} \frac{\alpha_s}{2\pi} P_{\tilde{ij}i}(z), \quad (3.5)$$

Note that the quantities  $S$  in this expression are symmetry factors, cf. Eq. (2.2). It is obvious that approximate higher-order corrections in successive collinear limits may be computed by simply iterating Eq. (3.5). In this process we would violate unitarity, as each integral contributes positively to the total cross section for the inclusive process described by  $d\sigma_n^{(B)}(\{\vec{a}\})$ . The solution is to add approximate virtual corrections, which are assumed to cancel exactly the real-emission corrections computed above. At the same time, a cutoff scale,  $t_c$ , is introduced, which ensures that no partonic process is computed below distances of order  $\Lambda_{\text{QCD}}$ . The virtual corrections and unresolved emissions below  $t_c$  can then be combined into the total contribution from unresolved emissions and virtual corrections. In the simplest case of a single radiating quark line, like in  $e^+e^- \rightarrow q\bar{q}$ , we obtain:

$$\sum_{m=0}^{\infty} \frac{1}{m!} \left[ - \int_{t_c} dt \int dz \frac{1}{2 p_i p_j} \frac{\alpha_s}{2\pi} P_{qq}(z) \right]^m = \exp \left\{ - \int_{t_c} dt \int dz \frac{1}{2 p_i p_j} \frac{\alpha_s}{2\pi} P_{qq}(z) \right\}. \quad (3.6)$$

In full generality, this contribution reads

$$\Pi_n^{\tilde{ij}, \tilde{k}}(t, t'; \{\vec{a}\}) = \exp \left\{ - \frac{1}{16\pi^2} \sum_{f_i \in \{q, g\}} \int_t^{t'} d\bar{t} \int dz \int \frac{d\phi}{2\pi} \frac{1}{2} \frac{S_{n+1}^{ij,k}(r_{\tilde{ij}, \tilde{k}}(f_i, \bar{t}, z, \phi; \{\vec{a}\}))}{B_n(\{\vec{a}\})} \right\}. \quad (3.7)$$

In the sum over all possible splittings, we obtain the no-branching probability of the parton shower:<sup>4</sup>

$$\Pi_n(t, t'; \{\vec{a}\}) = \prod_{\{\tilde{ij}, \tilde{k}\}} \Pi_n^{\tilde{ij}, \tilde{k}}(t, t'; \{\vec{a}\}). \quad (3.8)$$

It represent the probability for no parton branching to occur between the scales  $t'$  and  $t$ . The probability for any parton to branch at scale  $t$  with evolution starting at  $t'$  is then given by Poisson statistics:

$$\mathcal{P}_1(t, t') = \frac{d\Pi_n(t, t'; \{\vec{a}\})}{d \log t}. \quad (3.9)$$

Parton showers solve this equation for  $t$  using the veto algorithm, which can be thought of as an extension of the hit-or-miss Monte-Carlo method to Poisson distributions [49]. In order to do this, a suitable starting scale for the evolution must be defined, which will be called the resummation scale in the following.

<sup>4</sup> In pure final-state parton evolution the no-branching probability  $\Pi_n^{\tilde{ij}, \tilde{k}}$  is equivalent to the Sudakov form factor, because the ratio of parton luminosities,  $\mathcal{L}(r_{\tilde{ij}, \tilde{k}}(f_i, t, z, \phi; \{\vec{a}\}))/\mathcal{L}(\{\vec{a}\})$  is precisely one.

This scale may be identified with the factorization scale. After  $t$  has been selected in the Monte-Carlo procedure, a value for the splitting variable and the azimuthal angle is found using standard Monte-Carlo techniques.

We can phrase the complete parton shower evolution in term of a generating functional,  $\mathcal{F}(t; \{\vec{a}\})$ , such that the expectation value of an observable,  $O$ , is computed as

$$\langle O \rangle^{(\text{PS})} = \sum_{\{\vec{f}\}} \int d\vec{\Phi}_n(\{\vec{p}\}) \bar{B}_n(\{\vec{a}\}) \mathcal{F}_n(\mu_Q^2; \{\vec{a}\}, O) . \quad (3.10)$$

The generating functional is recursively defined as

$$\begin{aligned} \mathcal{F}_n(\mu_Q^2; \{\vec{a}\}, O) &= \underbrace{\Pi_n(t_c, \mu_Q^2; \{\vec{a}\})}_{\text{virtual+unresolved}} O(\{\vec{p}\}) \\ &+ \sum_{\{\vec{i}, \vec{k}\}} \sum_{f_i=q,g} \int d\Phi_{+1}^{ij,k} \Theta(t(\Phi_{+1}^{ij,k}) - t_c) \\ &\times \underbrace{\frac{1}{S_{ij}} \frac{S(r_{\vec{i}, \vec{k}}(f_i; \{\vec{f}\}))}{S(\{\vec{f}\})} \frac{D_{n+1}^{ij,k}(r_{\vec{i}, \vec{k}}(f_i, \Phi_{+1}^{ij,k}; \{\vec{a}\}))}{B_n(\{\vec{a}\})}}_{\text{resolved}} \Pi_n(t, \mu_Q^2; \{\vec{a}\}) \\ &\times \mathcal{F}_{n+1}(t; r_{\vec{i}, \vec{k}}(f_i, \Phi_{+1}^{ij,k}; \{\vec{a}\}), O) . \end{aligned} \quad (3.11)$$

The first term is the resummed contribution from virtual and unresolved real-emission corrections, while the second term comes from a single real-emission and the resummed virtual and unresolved corrections between the hard scale and the scale of the emission.  $S_{ij}$  is a symmetry factor in the shower approximation. We have replaced the dipole subtraction terms by a new function,  $D_{n+1}^{ij,k}$ , which accounts for the fact that the parton-shower evolution kernels typically do not implement the spin and color correlations that are present in Eq. (2.31). Further emissions may occur after the first, which is implemented by the generating functional  $\mathcal{F}_{n+1}$  on the last line. Expanding this formula up to first emission only,  $\mathcal{F}_{n+1}$  would turn into  $O_{n+1}$ , which is used in some literature on matching [38, 39].

### 3.2 The veto algorithm

Equation (3.9) is difficult to solve with Monte-Carlo methods if the integral of the splitting functions is not known analytically. In practice, this is most often the case. One reason is that the evolution kernels may not be simple Altarelli-Parisi splitting functions but more complicated expressions. Another reason is that the integral may be hard to compute for a given functional form of the evolution variable  $t$  and the phase-space boundaries imposed by local four-momentum conservation. It would be simpler to find an overestimate of the integrand and perform a hit-or-miss Monte-Carlo integration. However, this is hampered by the fact that we intend to evaluate an integral in the exponent. The solution to this problem lies in using the Sudakov veto algorithm.

To simplify the notation, let  $f(t)$  be the splitting kernel of the parton shower, integrated over the splitting variable  $z$ . We also assume that only one splitting function exists, i.e. that there is no flavor change of the splitter during the evolution. The differential probability for generating a single branching at scale  $t$  when starting from an upper evolution scale  $t'$  is then given by

$$\mathcal{P}_1(t, t') = f(t) \exp \left\{ - \int_t^{t'} d\bar{t} f(\bar{t}) \right\} = \frac{d}{dt} \exp \left\{ - \int_t^{t'} d\bar{t} f(\bar{t}) \right\} . \quad (3.12)$$

A new scale  $t$  can in principle be determined as

$$t = F^{-1} [F(t') + \log R] \quad \text{where} \quad F(t) = \int_t^t dt f(t) , \quad (3.13)$$



and where  $R$  is a random number between zero and one. The key point of the veto algorithm is, that even if the integral  $F(t)$  is unknown, one can still generate events according to  $\mathcal{P}$  using an overestimate  $g(t) \geq f(t)$  with a known integral  $G(t)$ . First, a value  $t$  is generated as  $t = G^{-1}[G(t') + \log R]$ . Second, the value is accepted with probability  $f(t)/g(t)$ . A splitting at  $t$  with  $n$  intermediate rejections is then produced with differential probability

$$\mathcal{P}_1^{(n)}(t, t') = \frac{f(t)}{g(t)} g(t) \exp \left\{ - \int_t^{t_1} d\bar{t} g(\bar{t}) \right\} \times \prod_{i=1}^n \left[ \int_{t_{i-1}}^{t_{i+1}} dt_i \left( 1 - \frac{f(t_i)}{g(t_i)} \right) g(t_i) \exp \left\{ - \int_{t_i}^{t_{i+1}} d\bar{t} g(\bar{t}) \right\} \right], \quad (3.14)$$

where  $t_{n+1} = t'$  and  $t_c = t$ . The nested  $t_i$ -integrals in Eq. (3.14) can be symmetrized, which leads to a symmetry factor  $1/n!$ . The exponentials can be combined into a single term where the  $\bar{t}$ -integral runs from  $t$  to  $t'$ . Summing over all possibilities for the number of intermediate rejections,  $n$ , then leads to the exponentiation of a factor  $g(t) - f(t)$ , such that Eq. (3.12) is reproduced [49].

### 3.3 Coherent branching

Up to this point we have not chosen the precise form of the splitting kernels in Eq. (3.7). Assume that we use the Altarelli-Parisi splitting functions,  $P_{ij}(z)$ .  $P_{qq}(z)$  is soft-enhanced when  $z \rightarrow 1$ . However, it does not differentiate between a situation where the soft gluon is radiated in the direction of the initial quark or in the direction of the spectator. When considering all radiating partons in the process, a naive integration over the full phase space available to soft gluon radiation would therefore lead to double counting of logarithmically enhanced soft (but not collinear) contributions. This can be circumvented using either an appropriate evolution variable or a variant of the splitting kernel which includes a regulator that damps the soft singularity in the anti-collinear region of the emission phase space.

Let us investigate this picture in more detail in  $e^+e^-$ -annihilation to hadrons. The differential cross section for  $e^+e^- \rightarrow q\bar{q}g$  is given by the QCD “antenna” radiation pattern

$$d\sigma_3 = d\sigma_2 \frac{dw}{w} \frac{d\Omega}{2\pi} C_F W_{q\bar{q}}^g, \quad \text{where} \quad W_{q\bar{q}} = \frac{1 - \cos \theta_{q\bar{q}}}{(1 - \cos \theta_{qg})(1 - \cos \theta_{\bar{q}g})}. \quad (3.15)$$

We can split the antenna  $W_{q\bar{q}}$  into two parts,  $W_{q\bar{q}}^{(q)}$  and  $W_{q\bar{q}}^{(\bar{q})}$ , which are divergent only if the gluon is collinear to the quark / antiquark:

$$W_{q\bar{q}} = W_{q\bar{q}}^{(q)} + W_{q\bar{q}}^{(\bar{q})}, \quad \text{where} \quad W_{q\bar{q}}^{(q)} = \frac{1}{2} \left( W_{q\bar{q}} + \frac{1}{1 - \cos \theta_{qg}} - \frac{1}{1 - \cos \theta_{\bar{q}g}} \right). \quad (3.16)$$

Upon azimuthal integration, we obtain [50]

$$\frac{d\phi_{qg}}{2\pi} W_{q\bar{q}}^{(q)} = \begin{cases} \frac{1}{1 - \cos \theta_{qg}} & \text{if } \theta_{qg} < \theta_{q\bar{q}} \\ 0 & \text{else} \end{cases}. \quad (3.17)$$

This is known as angular ordering: The gluon can only be emitted inside the cone spanned by the initial directions of the quark/antiquark. If it is emitted outside, it cannot resolve the individual color charges of the quarks.

For processes with more final-state partons the situation becomes slightly more complicated. A convenient method to analyze the situation is to work with color charge operators  $\mathbf{T}$ , cf. (2.30). This amounts to analyzing the combined color charge, which leads to emission of QCD radiation off a parton pair. The color charge operators squared give the Casimir operators,  $\mathbf{T}_i^2 = C_F$ , if  $i$  is a quark and  $\mathbf{T}_i^2 = C_A$ , if  $i$  is a gluon. For color singlets,  $\mathbf{T}_i^2$  vanishes. Each antenna multiplies a corresponding color-charge operator, such that the full contribution from the radiating “color dipole” formed by partons  $i$  and  $j$  reads

$$\mathbf{W}_{ij} = -\mathbf{T}_i \cdot \mathbf{T}_j W_{ij}. \quad (3.18)$$

In electron-positron annihilation into quarks, this corresponds exactly to the situation discussed above. Consider now the radiation from a three-parton final state. The radiation pattern is then given by

$$\begin{aligned} \mathbf{W}_{ijk} &= -\mathbf{T}_i \cdot \mathbf{T}_j W_{ij} - \mathbf{T}_j \cdot \mathbf{T}_k W_{jk} - \mathbf{T}_k \cdot \mathbf{T}_i W_{ik} \\ &= \frac{1}{2} \left[ \mathbf{T}_i^2 (W_{ij} + W_{ik} - W_{jk}) + \mathbf{T}_j^2 (W_{jk} + W_{ij} - W_{ik}) + \mathbf{T}_k^2 (W_{ik} + W_{jk} - W_{ij}) \right]. \end{aligned} \quad (3.19)$$

If  $i$  and  $j$  are close to each other they form a combined system  $l$ , which carries the net color charge  $\mathbf{T}_i + \mathbf{T}_j = \mathbf{T}_l$ . For small angles between  $i$  and  $j$ ,  $W_{ik} \approx W_{jk} \approx W_{lk}$ . Equation (3.19) can then be written as [50]

$$\mathbf{W}_{ijk} \approx \mathbf{T}_i^2 W_{ij}^{(i)} + \mathbf{T}_j^2 W_{ij}^{(j)} + \mathbf{T}_k^2 W_{lk}^{(k)} + \mathbf{T}_l^2 \tilde{W}_{lk}^{(l)} \Theta(\theta_{lg} - \theta_{ij}). \quad (3.20)$$

This equation has again a simple interpretation. Each parton itself radiates proportional to its color charge squared, while additional radiation comes from coherent emission off the parton pair  $ij$  if the emission angle  $\theta_{lg}$  exceeds the opening angle  $\theta_{ij}$  of the pair. The partons then radiate proportional to their combined color charge squared,  $\mathbf{T}_l^2$ . The formalism may be extended to higher multiplicity, and leads to the coherent-branching formalism. It can be interpreted as an angular-ordering constraint for the partons emitted in each step of a parton shower.

In the parton shower implemented in Herwig, this angular ordering constraint is realized through the choice of evolution variable. Alternatively, it may be implemented by using Eq. (3.16) instead of the sum of two Altarelli-Parisi kernels used in standard parton showers. This choice was first advocated in the linked dipole chain model [51]. Partial fractioning the antenna and assigning each term the meaning of a splitting function in the presence of a spectator parton leads to yet another option for implementing effective angular ordering. This is the option we have chosen to introduce the generic parton-shower model above, because it allows one to retain the notion of a splitter parton, which can be associated with the collinear direction in the collinear limit.

Schematically, this partial fractioning is performed as [13]

$$\frac{p_i p_k}{(p_i p_j)(p_j p_k)} \rightarrow \frac{1}{p_i p_j} \frac{p_i p_k}{(p_i + p_k) p_j} + \frac{1}{p_k p_j} \frac{p_i p_k}{(p_i + p_k) p_j}. \quad (3.21)$$

The terms  $1/(p_i p_j)$  and  $1/(p_k p_j)$  lead to double-collinear singularities, while the remaining terms do not contain any two-particle poles. Only the soft singularity structure is reflected by Eq. (3.21). The spin-dependent terms of the collinear splitting functions are added explicitly, leading to the Catani-Seymour dipole splitting functions [13]. In a parton shower, they are mostly used in their spin-averaged form, which reads

$$\begin{aligned} \langle V \rangle_{qq}(\tilde{z}, y) &= C_F \left[ \frac{2}{1 - \tilde{z}(1 - y)} - (1 + \tilde{z}) \right], \\ \langle V \rangle_{gg}(\tilde{z}, y) &= 2C_A \left[ \frac{1}{1 - \tilde{z}(1 - y)} + \frac{1}{1 - (1 - \tilde{z})(1 - y)} - 2 + \tilde{z}(1 - \tilde{z}) \right]. \end{aligned} \quad (3.22)$$

Note that  $\langle V \rangle_{qq}(\tilde{z}, y) = P_{qq}(\tilde{z})$ , as no soft gluon singularity needs to be taken care of. The variable  $y$  is given by  $y = (p_i p_j)/(p_i p_j + p_i p_k + p_j p_k)$ , while the light-cone momentum fraction  $\tilde{z}$  is defined as  $\tilde{z} = (p_i p_k)/(p_i p_k + p_j p_k)$ , cf. Sec. 1.4.

### 3.4 The large- $N_C$ approximation

Parton showers as Markov-Chain Monte-Carlo algorithms build on the assumption that the Sudakov factors in Eq. (3.8) are positive numbers, which represent the probability for a parton not to undergo branching between two scales. This makes it difficult to accommodate full color coherence, as the color dipoles discussed above radiate proportional to their color correlators  $-\mathbf{T}_i \mathbf{T}_k$ . These terms may be negative, which would lead to non-probabilistic Sudakov factors. This situation can be dealt with in principle [52, 53, 15], and several algorithms have been proposed to accommodate the non-probabilistic

	Evolution variable	Splitting variable	Coherence	Reference
Ariadne	dipole- $k_{\perp}^2$	Rapidity	Antenna	[62, 51, 63]
Dire	dipole- $k_{\perp}^2$	LC mom fraction	Dipole	[64]
Herwig	$E^2\theta^2$	Energy fraction	AO	[65, 66]
Herwig++	$(t - m^2)/z(1 - z)$	LC mom fraction	AO/Dipole	[67, 68]
Pythia <6.4	$t$	Energy fraction	Enforced	[69, 70]
Pythia $\geq 6.4$	$k_{\perp}^2$	LC mom fraction	Enforced	[71]
Sherpa <1.2	$t$	Energy fraction	Enforced	[72]
Sherpa $\geq 1.2$	$k_{\perp}^2$	LC mom fraction	Dipole	[73]
Vincia	variable	variable	Antenna	[74, 75]

**Table 1:** Choice of evolution/splitting variable and evolution kernels in common parton-shower programs.

terms in the veto algorithm [53, 54]. The much more common solution, however, is to use an approximation similar to the large- $N_C$  approximation.

In the large- $N_C$  limit, color-octet gluons are replaced by a color triplet-antitriplet pair.  $1/N_C$  terms are absent, leading to a simple color topology consisting of a planar flow. Each branching creating a gluon in the final state leads to a new “color”, and each gluon (quark) is connected to two and only two (one and only one) other parton. QCD radiation in this approximation is always simulated as the radiation from a single color dipole, rather than a coherent sum from a color multipole. However, the color charge for radiation off quarks is still set by  $C_F$ , and not by  $N_C/2$ . This accounts for the leading  $1/N_C$  effects, and it matches the result obtained by color conservation in the collinear limit.

### 3.5 Practical implementation

Up to now we have not specified the precise form of the evolution variable,  $t$ . If we choose the propagator virtuality,  $dt/(2p_i p_j)$  becomes a logarithmic integral. At this point, we can perform arbitrary variable transformations without introducing additional Jacobian factors. In other words, the evolution variables virtuality, transverse momentum, and polar angle are all formally equivalent, because

$$\frac{dt}{t} = \frac{dk_T^2}{k_T^2} = \frac{dq_T^2}{q_T^2}, \quad (3.23)$$

where  $q_T = -t/(1 - z)$  for initial-state and  $q_T = t/(z(1 - z))$  for final-state splittings, while  $k_T^2$  is the relative transverse momentum in the branching process. We have seen in Sec. 3.3 that angular ordering can effectively model color coherence, and it might therefore be preferred as an evolution variable, as long as the evolution kernels are given by the Altarelli-Parisi splitting functions.

While resumming universal higher-order corrections to the hard process, parton showers are themselves derived only from the leading real-emission corrections. There are, however, universal higher-order terms which must be taken into account to make the parton-shower prediction meaningful: The first is the universal coupling renormalization, which leads to corrections of the form  $\alpha_s/(2\pi)\beta_0 \log(k_T^2/\mu_R^2)$ , where  $k_T^2$  is again the relative transverse momentum in the gluon emission [55, 56, 57, 58, 59, 60]. This term can be absorbed into the running coupling, leading to a particular scale choice which is different for each branching and depends on the splitting kinematics:  $\alpha_s(k_T^2)$ . The other universal term to be incorporated relates the unphysical  $\overline{\text{MS}}$  renormalization scheme to a physical scheme, by including the two-loop cusp anomalous dimension,  $K = (67/18 + \zeta_2)C_A - 10/9 T_R n_f$ , into the soft-enhanced terms of the splitting functions [61]. As the term may equally well be absorbed into the scale of the running coupling, this method is also referred to as the CMW scale choice.

The choices made in presently-available parton shower programs are listed in Tab. 1. The quality of a certain choice of splitting parameters can often be judged only after comparing the results of the simulation to experimental measurements.

## 4 Matching and Merging

Parton showers implement approximate higher-order real-emission corrections to arbitrary hard processes using the universal soft and collinear factorization properties of the hard cross sections. They estimate virtual corrections through unitarity conditions. In order to improve the description of observables, it is often necessary to go beyond these approximations. One possibility in so doing is to replace the parton shower approximation at given orders in the strong coupling expansion by exact perturbative QCD results. This can be done in two different ways.

- *Matching*

The parton-shower expression at fixed order is computed and subtracted from the higher-order calculation to remove double counting. The subtracted result is processed by the parton shower.

- *Merging*

A separate tree-level calculation is performed for each parton multiplicity of interest. Soft and collinear divergences of the hard matrix elements are regulated by resolution cuts. The parton shower is combined with all these calculations, and double-counting is removed by appropriate vetoes on shower branchings.

The concept of infrared-safe observables and QCD jets plays a crucial role for merging. Both the initial state and many final states at hadron colliders include hard partons. Initial- and final-state Bremsstrahlung dress these partons with further radiation. The new particles are found predominantly in the vicinity of the original ones, leading to clusters of radiation called QCD jets. The hadronization mechanism preserves the jet structure, such that it can be observed experimentally. Theoretically, a cluster of hadronic energy can thus be identified with one or more hard initiating partons. For this concept to work an algorithm must be defined which unambiguously relates the two scenarios. Crucially, this algorithm must be infrared and collinear safe: if a single parton is replaced with a set of collinear partons sharing its original energy, the jet configuration must not change. Likewise, if a soft parton is added to the original jet configuration, the jet configuration according to the jet algorithm must not change. Reviews of jet algorithms are provided elsewhere [14]. In the following we will make use of jets only as theoretical tools for the merging of parton showers with multiple higher-order tree-level calculations.

### 4.1 Matching

Using the subtraction formalism introduced in Sec. 2.4, an arbitrary infrared and collinear safe observable can be computed at NLO QCD as

$$\begin{aligned} \langle O \rangle^{(\text{NLO})} = & \sum_{\{\vec{f}\}} \int d\bar{\Phi}_n(\{\vec{p}\}) \left( B_n(\{\vec{a}\}) + \tilde{V}_n(\{\vec{a}\}) + \sum_{\{\vec{ij}, \vec{k}\}} I_n^{\vec{ij}, \vec{k}}(\{\vec{a}\}) \right) O(\{\vec{p}\}) \\ & + \sum_{\{\vec{f}\}} \int d\bar{\Phi}_{n+1}(\{\vec{p}\}) \left( B_{n+1}(\{\vec{a}\}) O(\{\vec{p}\}) - \sum_{\{\vec{ij}, \vec{k}\}} S_{n+1}^{ij, k}(\{\vec{a}\}) O(b_{ij, k}(\{\vec{p}\})) \right). \end{aligned} \quad (4.1)$$

Note that the configurations  $\{\vec{f}\}$ ,  $\{\vec{p}\}$  and  $\{\vec{a}\}$  on the second line each include one more particle than the term on the first line, because they represent the real-emission momentum and flavor configuration. The infrared and collinear safety of the observable guarantees that the expectation value computed in this manner is physically meaningful.

We now subtract the parton-shower approximation of the NLO result, which consists of the resolved real-emission corrections, and the unresolved corrections (virtual and real-emission contribution below  $t_c$ ). To distinguish the parton-shower expression from the original subtraction terms, and because the actual form of the dipole terms used in the parton shower may differ, we call these contributions  $D(\{\vec{a}\})$ . We also re-order the real-emission term according to the principles in Sec. 3:

$$\sum_{\{\vec{f}\}} \int d\bar{\Phi}_n(\{\vec{p}\}) \bar{B}_n(\{\vec{a}\}) O(\{\vec{p}\}) + \sum_{\{\vec{f}\}} \int d\bar{\Phi}_{n+1}(\{\vec{p}\}) H_{n+1}(\{\vec{a}\}) O(\{\vec{p}\}), \quad (4.2)$$

The function  $\bar{B}(\{\vec{a}\})$  represents the NLO cross section differential in the phase space of the Born process, up to a hard correction. We will call this term the NLO-weighted Born differential cross section. The function  $H_{n+1}(\{\vec{a}\})$  represents the difference between the real-emission correction and the parton-shower approximation, expanded to first order in the strong coupling:

$$\begin{aligned} \bar{B}_n(\{\vec{a}\}) &= B_n(\{\vec{a}\}) + \tilde{V}_n(\{\vec{a}\}) + \sum_{\{\tilde{ij}, \tilde{k}\}} I_n^{\tilde{ij}, \tilde{k}}(\{\vec{a}\}) \\ &\quad + \sum_{\{\tilde{ij}, \tilde{k}\}} \sum_{fi=q,g} \int d\Phi_{+1}^{ij,k} \left[ D_{n+1}^{ij,k}(r_{\tilde{ij}, \tilde{k}}(\{\vec{a}\})) - S_{n+1}^{ij,k}(r_{\tilde{ij}, \tilde{k}}(\{\vec{a}\})) \right] \end{aligned} \quad (4.3)$$

$$H_{n+1}(\{\vec{a}\}) = B_{n+1}(\{\vec{a}\}) - \sum_{\{ij,k\}} D_{n+1}^{ij,k}(\{\vec{a}\}) .$$

Equation (4.2) alone cannot be used to compute physical observables, because of the non-local nature of the subtraction. Once the parton shower is added, this mismatch is canceled to NLO accuracy, and only corrections of higher-order in the strong coupling expansion remain. The first working proposal for NLO matching, MC@NLO, is therefore also called a modified subtraction method [37]. The full matched result reads

$$\begin{aligned} \langle O \rangle^{(\text{NLOMC})} &= \sum_{\{\vec{f}\}} \int d\bar{\Phi}_n(\{\vec{p}\}) \bar{B}_n(\{\vec{a}\}) \mathcal{F}_n(\mu_Q^2; \{\vec{a}\}, O) \\ &\quad + \sum_{\{\vec{f}\}} \int d\bar{\Phi}_{n+1}(\{\vec{p}\}) H_{n+1}(\{\vec{a}\}) \mathcal{F}_{n+1}(\mu_Q^2; \{\vec{a}\}, O) . \end{aligned} \quad (4.4)$$

$\mathcal{F}_{n+1}(\mu_Q^2)$  is defined in the sense of a truncated parton shower, which will be discussed in Sec. 4.2. Expanded up to the first emission, we obtain the formula used to describe the POWHEG method [38, 39]

$$\begin{aligned} \langle O \rangle^{(\text{NLOMC})} &\rightarrow \sum_{\{\vec{f}\}} \int d\bar{\Phi}_n(\{\vec{p}\}) \bar{B}_n(\{\vec{a}\}) \left[ \underbrace{\Pi_n(t_c, \mu_Q^2; \{\vec{a}\})}_{\text{virtual+unresolved}} O(\{\vec{p}\}) \right. \\ &\quad + \sum_{\{\tilde{ij}, \tilde{k}\}} \sum_{fi=q,g} \int d\Phi_{+1}^{ij,k} \Theta(t(\Phi_{+1}^{ij,k}) - t_c) O(r_{\tilde{ij}, \tilde{k}}(\Phi_{+1}^{ij,k}; \{\vec{p}\})) \\ &\quad \times \underbrace{\frac{1}{S_{ij}} \frac{S(r_{\tilde{ij}, \tilde{k}}(f_i; \{\vec{f}\}))}{S(\{\vec{f}\})} \frac{D_{n+1}^{ij,k}(r_{\tilde{ij}, \tilde{k}}(f_i, \Phi_{+1}^{ij,k}; \{\vec{a}\}))}{B_n(\{\vec{a}\})} \Pi_n(t, \mu_Q^2; \{\vec{a}\})}_{\text{resolved, singular}} \left. \right] \\ &\quad + \sum_{\{\vec{f}\}} \int d\bar{\Phi}_{n+1}(\{\vec{p}\}) \left[ \underbrace{B_{n+1}(\{\vec{a}\}) - \sum_{ij,k} D_{n+1}^{ij,k}(\{\vec{a}\})}_{\text{resolved, non-singular}} \right] O(\{\vec{p}\}) . \end{aligned} \quad (4.5)$$

Equation (4.4) can be used to describe the matching of NLO QCD calculations to parton showers in both the MC@NLO and POWHEG methods [37, 38, 39, 76]. Monte-Carlo events are generated in the following way.

- A seed event is produced according to either the first or the second line of Eq. (4.2).
- If the second line is chosen, the event has real-emission kinematics and is kept as-is. This generates the “resolved, non-singular” term of Eq. (4.4). Such events are called hard remainder events, or  $\mathbb{H}$ -events.
- If the first line is chosen, the event has Born-like kinematics and is processed by the parton shower. Such events are called standard events, or  $\mathbb{S}$ -events. An emission might or might not occur, as indicated by the “resolved, singular” and “unresolved” terms of Eq. (4.4).

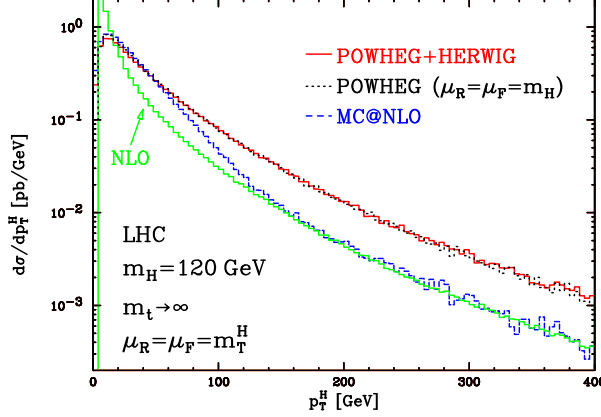


**Figure 5:** Comparison of predictions from MC@NLO and POWHEG for the transverse momentum of the Higgs boson in inclusive Higgs-boson production. Figure taken from [78].

For this method to work in processes with non-trivial color structure, it is vital that the dipole terms used in the shower,  $D_{n+1}^{ij,k}$ , have the exact same soft and collinear limits as the real-emission matrix elements. Otherwise the hard remainder contribution will be divergent, as will the NLO weighted Born differential cross section. Typical parton showers, however, do not correctly account for the soft singularities in processes with non-trivial color structure at Born level (cf. Sec. 3.4). The problem can be solved by adding a soft-suppression factor to both the second line in Eq. (4.3) and the second line in Eq. (4.2) [37]. Alternatively, one may correct the parton-shower approximation with the exact dipole terms as defined by Eq. (2.31), which necessitates the computation of non-probabilistic Sudakov factors [53, 54].

Note that Eq. (4.4) describes only a single parton-shower step. In principle one can therefore change the parton-shower generator after the matching has been performed. This idea is used in the POWHEG method [38, 39], which can be thought of as a matching to a matrix-element corrected parton shower. In this case the parton-shower dipoles are defined as:

$$D_{n+1}^{ij,k} \rightarrow \rho_{ij,k}(\{\vec{a}\}) B_{n+1}(\{\vec{a}\}) \quad \text{where} \quad \rho_{ij,k}(\{\vec{a}\}) = \frac{\mathcal{D}_{n+1}^{ij,k}(\{\vec{a}\})}{\sum_{mn,l} \mathcal{D}_{n+1}^{mn,l}(\{\vec{a}\})}. \quad (4.6)$$

This means the full radiative corrections are exponentiated into a Sudakov form factor. After the first emission (or no-emission), the parton shower is used to implement further splittings.

One can construct a mixed scheme, where  $D_{n+1}^{ij,k}$  is defined as

$$D_{n+1}^{ij,k} \rightarrow \rho_{ij,k}(\{\vec{a}\}) \left[ B_{n+1}(\{\vec{a}\}) - B_{n+1}^{(r)}(\{\vec{a}\}) \right], \quad (4.7)$$

with  $R^{(r)}$  an arbitrary infrared-finite part of the real-emission cross section and  $\rho_{ij,k}$  given by Eq. (4.6). This method can be used in particular to deal with the problem of zeros in the Born process [77].

Figure 5 shows a comparison between predictions from MC@NLO [37] and POWHEG [38, 39] for the transverse momentum spectrum of the Higgs boson in inclusive Higgs-boson production. The MC@NLO result shows a feature around the resummation scale,  $\mu_Q = 120 \text{ GeV}$ , while the POWHEG result does not. This can be attributed to the large NLO  $K$ -factor in this process, which multiplies the NLO-weighted Born cross section, Eq. (4.3). In the MC@NLO method, this contribution generates resolved radiation only up to a transverse momentum of  $\mu_Q$ , cf. Eq. (4.4). In contrast, in the original POWHEG method shown here it generates radiation up to the hadronic center of mass energy, as  $\mu_Q \rightarrow E_{\text{cms}}$ . The difference between the full matrix-element corrections used in POWHEG (cf. Eq. (4.6)) and the DGLAP splitting kernels used in MC@NLO has a much smaller effect.

This example demonstrates that NLO matching techniques do not account for all possible higher-order effects, as the matching condition only guarantees the preservation of NLO and parton-shower accu-

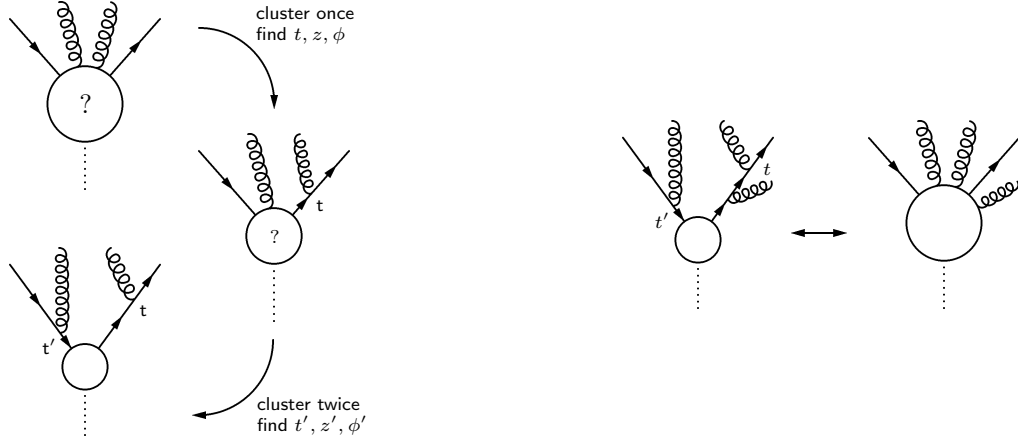


**Figure 6:** Left: Sketch of a clustering sequence identifying the  $e^+e^- \rightarrow q\bar{q}$  inclusive reaction in a  $e^+e^- \rightarrow q\bar{q}gg$  final state. Right: Sketch of a truncated parton-shower emission in the existing history and its correspondence to the higher-order tree-level matrix element.

racy. If higher-order corrections to the process are still large, as in the case of Higgs-boson production, improvements to NLO matching must be found.

## 4.2 Merging

Merging algorithms combine tree-level calculations for multi-jet configurations with parton showers. In this context, the leading-order calculation must be interpreted in terms of a parton-shower branching history, in order to identify the Sudakov factors that need to be included in order to maintain (approximate) unitarity of the inclusive cross section. It is therefore vital that the parton shower is invertible, in other words, that any particular  $(n+k)$ -particle final state can be mapped onto the  $n$ -particle final state of the inclusive process by successive recombination of two partons into one. This is sketched in Fig. 6 (left). At each step of the clustering four-momentum is conserved locally, according to the exact inverted parton-shower kinematics. Standard parton showers have multiple coverage of the full phase space through different splitting processes, and therefore several possible clustered configurations exist for one and the same final state. To obtain a definite configuration that can be used as a starting condition for the parton shower, the cluster algorithm must select one of the options with the correct probability.

Once a parton-shower “history” corresponding to the hard-scattering configuration has been identified, it is dressed with further radiation by the parton shower. Radiation can occur at any point in the configuration. This is exemplified in Fig. 6 (right), where the emission of a gluon from an intermediate quark propagator is sketched. The situation is called “truncated showering”, because the evolution is truncated at scale  $t$ , where radiation of the additional gluon already present in the hard scattering calculation must be re-implemented. At the same time, we need to test whether the newly-emitted parton is hard enough to constitute a jet on its own. In this case the configuration should be simulated using a hard-scattering calculation with one more jet, as indicated in Fig. 6 (right). To avoid double counting, the event with hard truncated showering must then be vetoed, which reduces the cross section and effectively generates a Sudakov factor for the evolution between the hard scale and the scale of jet resolution. This scale, called  $Q_{\text{cut}}$ , is a technical parameter of the merging algorithm, and the dependence of the final result on it must cancel to the logarithmic accuracy of the parton shower.

To formalize the above ideas we first introduce  $Q_{\text{cut}}$  as a criterion for the real-emission configuration to be of  $l$ -jet type. For final states with  $(n+l+1)$  particles, we identify an  $(n+l)$ -particle final state by clustering according to the kinematics and probability defined by the parton shower. We define the  $l$ -jet

inclusive and exclusive expectation values

$$\begin{aligned}\langle O \rangle_l^{\text{incl}} &= \sum_{k=0}^{\infty} \langle O_{l+k} \Theta(Q_{l+k} - Q_{\text{cut}}^l) \rangle, \\ \langle O \rangle_l^{\text{excl}} &= \sum_{k=0}^{\infty} \langle O_{l+k} \Theta(Q_{l+k} - Q_{\text{cut}}^l) \Theta(Q_{\text{cut}}^l - Q_{l+k+1}) \rangle.\end{aligned}\tag{4.8}$$

They include contributions from all final states with at least  $l$  partons, which must form  $l$  (but not  $l+1$  in the case of  $\langle O \rangle_l^{\text{excl}}$ ) parton-level jets according to the definition of the jet resolution criterion  $Q$ . Note that the identification of jet configurations is used only to separate the phase space for hard QCD radiation into regions described by different hard matrix elements. Eventually, a fully inclusive simulation will be obtained by summing all jet configurations as

$$\langle O \rangle = \sum_{l=0}^{N_{\text{max}}-1} \langle O \rangle_l^{\text{excl}} + \langle O \rangle_{N_{\text{max}}}^{\text{incl}}.\tag{4.9}$$

$N_{\text{max}}$  is the highest possible jet multiplicity that can practically be computed using the matrix-element generator. It depends on the order of the hard-scattering calculation and on the process, and typically ranges between 4 and 6 for LO calculations and 2 and 3 for NLO calculations.

If the parton shower were to evolve only the final state, and not any of the intermediate states, we would obtain, after the first emission,

$$\langle O \rangle_l^{\text{excl}} \rightarrow \sum_{\{\vec{f}\}} \int d\bar{\Phi}_{n+l} B_{n+l} \Theta(Q_{n+l} - Q_{\text{cut}}^l) \Pi_m(t_c, \mu_Q^2; > Q_{\text{cut}}^{l+1}) \mathcal{F}_{n+l}(\mu_Q^2; O, < Q_{\text{cut}}^{l+1}).\tag{4.10}$$

For ease of notation we dropped the arguments  $\{\vec{a}\}$ ,  $\{\vec{f}\}$ , and  $\{\vec{p}\}$ . From here on we also drop the explicit notation of the kinematics mappings,  $b_{ij,k}(\{\vec{a}\})$  and  $r_{\tilde{i},\tilde{k}}(\{\vec{a}\})$ . In addition we define Sudakov factors for the vetoed parton shower, using Eq. (3.8) and

$$\begin{aligned}\Pi_m^{\tilde{i},\tilde{k}}(t, t'; > Q_{\text{cut}}^{l+1}) &= \exp \left\{ -\frac{1}{16\pi^2} \sum_{f_i \in \{q,g\}} \int_t^{t'} d\bar{t} \int dz \int \frac{d\phi}{2\pi} \right. \\ &\quad \left. \times \frac{1}{2} \frac{D_{m+1}^{ij,k}}{B_m} \Theta(Q_{m+1} - Q_{\text{cut}}^{l+1}) \right\}.\end{aligned}\tag{4.11}$$

We also introduce the vetoed generating functional

$$\begin{aligned}\mathcal{F}_m(\mu_Q^2; O, < Q_{\text{cut}}^{l+1}) &= \Pi_m(t_c, \mu_Q^2; < Q_{\text{cut}}^{l+1}) O_m + \sum_{\{\tilde{i},\tilde{k}\}} \sum_{f_i=q,g} \int d\Phi_{+1}^{ij,k} \Theta(t(\Phi_{+1}^{ij,k}) - t_c) \\ &\quad \times \frac{1}{S_{ij}} \frac{S_{m+1}}{S_m} \frac{D_{m+1}^{ij,k}}{B_m} \Pi_m(t, \mu_Q^2; < Q_{\text{cut}}^{l+1}) \Theta(Q_{\text{cut}}^{l+1} - Q_{m+1}) \mathcal{F}_{m+1}(t; O, < Q_{\text{cut}}^{l+1}).\end{aligned}\tag{4.12}$$

Unitarity requires that  $\mathcal{F}_m(\mu_Q^2; 1, < Q_{\text{cut}}^{l+1}) = 1$ . Therefore, the naive merging algorithm, Eq. (4.10), reduces the  $l$ -jet cross section computed by hard matrix elements by the factor  $\Pi_{n+l}(t_c, \mu_Q^2; > Q_{\text{cut}}^{l+1})$ . In other words, it turns the matrix-element result, which is an inclusive result for  $l$ -jet production, into an exclusive result by resumming the leading corrections from virtual and unresolved real-emission contributions. Qualitatively this observation holds also for the correct merging procedure.

Equation (4.10) does not take truncated showers into account and therefore violates the parton-shower evolution equations. To correct the problem without further complicating the notation, we extend our



definition of the parton shower evolution kernels:

$$\begin{aligned} \tilde{D}_{n+l+1} = & \sum_{\{\tilde{i}\tilde{j}, \tilde{k}\}, f_i} \frac{S_{n+l+1}}{S_{ij} S_{n+l}} D_{n+l+1}^{ij,k} \Theta(t_{n+k} - t) \\ & + B_{n+l} \sum_{m=n}^{n+l-1} \sum_{\{\tilde{i}\tilde{j}, \tilde{k}\}, f_i} \frac{S_{m+1}}{S_{ij} S_m} \frac{D_{m+1}^{ij,k}}{B_m} \Theta(t_m - t) \Theta(t - t_{m+1}) , \end{aligned} \quad (4.13)$$

Equation (4.13) is called the compound subtraction term. The  $\Theta$ -functions guarantee that the evolution kernel for the  $m$ -particle state is active only in the regions where the newly emitted particle has an evolution parameter,  $t$ , ranging between the ones in the previous and in the subsequent splitting. Only the evolution of the full final state proceeds unrestricted. We also define a compound Sudakov factor and the related generating functional of the parton shower:

$$\tilde{\Pi}_{n+l}(t, t') = \exp \left\{ - \frac{1}{16\pi^2} \int_t^{t'} d\bar{t} \int dz \int \frac{d\phi}{2\pi} \frac{\tilde{D}_{n+l+1}}{B_{n+l}} \right\} , \quad (4.14)$$

and

$$\tilde{\mathcal{F}}_{n+l}(\mu_Q^2; O) = \tilde{\Pi}_{n+l}(t_c, \mu_Q^2) O_{n+l} + \int_{t_c}^{\mu_Q^2} d\Phi_{+1} \frac{\tilde{D}_{n+l+1}}{B_{n+l}} \tilde{\Pi}_{n+l}(t, \mu_Q^2) \tilde{\mathcal{F}}_{n+l+1}(t; O) . \quad (4.15)$$

Correspondingly,  $\tilde{\mathcal{F}}_{n+l}(\mu_Q^2; O, < Q_{\text{cut}}^{l+1})$  is defined with an additional cut on the real-emission term, in complete analogy to Eq. (4.11). The  $l$ -jet contribution to  $O$  finally is

$$\langle O \rangle_l^{\text{excl}} = \sum_{\{\tilde{f}\}} \int d\tilde{\Phi}_{n+l} B_{n+l} \Theta(Q_{n+l} - Q_{\text{cut}}^l) \tilde{\Pi}_{n+l}(t_c, \mu_Q^2; > Q_{\text{cut}}^{l+1}) \tilde{\mathcal{F}}_{n+l}(\mu_Q^2; O, < Q_{\text{cut}}^{l+1}) . \quad (4.16)$$

Expanded up to the first emission, we have

$$\begin{aligned} \langle O \rangle_l^{\text{excl}} \rightarrow & \sum_{\{\tilde{f}\}} \int d\tilde{\Phi}_{n+l} B_{n+l} \Theta(Q_{n+l} - Q_{\text{cut}}^l) \tilde{\Pi}_{n+l}(t_c, \mu_Q^2; > Q_{\text{cut}}^{l+1}) \left[ \tilde{\Pi}_{n+l}(t_c, \mu_Q^2; < Q_{\text{cut}}^{l+1}) O_{n+l} \right. \\ & \left. + \int_{t_c}^{\mu_Q^2} d\Phi_{+1} \frac{\tilde{D}_{n+l+1}}{B_{n+l}} \tilde{\Pi}_{n+l}(t, \mu_Q^2; < Q_{\text{cut}}^{l+1}) \Theta(Q_{\text{cut}}^{l+1} - Q_{n+l+1}) O_{n+l+1} \right] . \end{aligned} \quad (4.17)$$

The logarithmic structure of the parton-shower is maintained by the merging only if the clustering procedure described above is an exact inversion of the shower evolution, and if truncated parton shower evolution, in particular the jet veto on the truncated shower emissions, is implemented. Note that if the hardness measure  $Q$  is identical to the evolution variable, truncated parton showers cannot produce an emission, but only lead to vetoes on events. A method to not implement truncated shower emissions while still maintaining formal accuracy and keeping the evolution variable and jet resolution parameter distinct also exists [79].

Note that Eq. (4.9) violates the unitarity of the parton-shower simulation, unless the splitting kernels used in the shower are given precisely by the real-emission matrix elements.<sup>5</sup> The reason for the unitarity violation is that we replaced resolved real-emission corrections by full tree-level matrix elements, while not accounting for the corresponding change in the unresolved and virtual corrections. This situation can be remedied by adding a correction to Eq. (4.16), which accounts for the difference in the unresolved region. Using the unitarity condition, the relevant terms can be computed with the same tree-level matrix elements which are also employed in the merging [80, 81].

The available merging schemes implemented in standard Monte-Carlo event generators are classified in Tab. 2. They differ in their use of parton showers, Sudakov factors (analytic/numerical) and jet resolution criterion. A thorough comparison of the available methods showed that their results are well comparable within the expected theoretical uncertainty [83].

<sup>5</sup>This case is irrelevant, because we would not need to perform any merging at all.

Method	Shower Generator	Unitary	Accuracy	References
MLM	Herwig/Pythia	No	unknown	[82, 83]
CKKW	Apacic	No	LO $\otimes$ PS	[84, 85]
CKKW-L	Ariadne/Pythia	No	LO $\otimes$ PS	[79, 86]
METS	Sherpa	No	LO $\otimes$ PS	[87]
CKKW'	Herwig++	No	LO $\otimes$ PS	[88]
UMEPS	Pythia	Yes	LO $\otimes$ PS	[80, 81]

**Table 2:** Practically implemented LO merging schemes.

### 4.3 Merging matched simulations

The merging methods described above can be extended to accommodate NLO calculations for the  $l$ -jet cross sections. In this process the matching must be modified, because the radiation probability of the full shower simulation has changed, and the  $\mathcal{O}(\alpha_s)$  expansion of the truncated parton shower approximation must be subtracted from the NLO result before it can be processed by the shower. This is done formally by defining the modified NLO-weighted Born cross section and the modified hard remainder:

$$\begin{aligned} \tilde{B}_{n+l} = & B_{n+l} + \tilde{V}_{n+l} + \sum_{\{\tilde{i}\tilde{j}, \tilde{k}\}} \tilde{I}_{n+l}^{\tilde{i}\tilde{j}, \tilde{k}} + \sum_{\{\tilde{i}\tilde{j}, \tilde{k}\}, f_i} \int d\Phi_{+1}^{ij,k} \left[ D_{n+l+1}^{ij,k} \Theta(t_{n+l} - t) - S_{n+l+1}^{ij,k} \right] \\ & + B_{n+l} \sum_{m=n}^{n+l-1} \sum_{\{\tilde{i}\tilde{j}, \tilde{k}\}, f_i} \int d\Phi_{+1}^{ij,k} \frac{D_{m+1}^{ij,k}}{B_m} \Theta(t_m - t) \Theta(t - t_{m+1}), \end{aligned} \quad (4.18)$$

$$\tilde{H}_{n+l+1} = B_{n+l+1} - \sum_{ij,k} D_{n+l+1}^{ij,k} \Theta(t_{n+l} - t) - B_{n+l} \sum_{m=n}^{n+l-1} \sum_{ij,k} \frac{D_{m+1}^{ij,k}}{B_m} \Theta(t_m - t) \Theta(t - t_{m+1}).$$

The  $l$ -jet contribution to the observable  $O$  from an NLO-calculation is then given by

$$\begin{aligned} \langle O \rangle_l^{\text{excl}} = & \sum_{\{\tilde{f}\}} \int d\bar{\Phi}_{n+l} \tilde{B}_{n+l} \Theta(Q_{n+l} - Q_{\text{cut}}^l) \tilde{\Pi}_{n+l}(t_c, \mu_Q^2; > Q_{\text{cut}}^{l+1}) \tilde{\mathcal{F}}_{n+l}(\mu_Q^2; O, < Q_{\text{cut}}^{l+1}) \\ & + \sum_{\{\tilde{f}\}} \int d\bar{\Phi}_{n+l+1} \tilde{H}_{n+l+1} \Theta(Q_{n+l} - Q_{\text{cut}}^l) \tilde{\Pi}_{n+l}(t_c, \mu_Q^2; > Q_{\text{cut}}^{l+1}) \tilde{\mathcal{F}}_{n+l+1}(\mu_Q^2; O, < Q_{\text{cut}}^{l+1}). \end{aligned} \quad (4.19)$$

Expanded up to the first emission, this becomes

$$\begin{aligned} \langle O \rangle_l^{\text{excl}} \rightarrow & \sum_{\{\tilde{f}\}} \int d\bar{\Phi}_{n+l} \tilde{B}_{n+l} \Theta(Q_{n+l} - Q_{\text{cut}}^l) \tilde{\Pi}_{n+l}(t_c, \mu_Q^2; > Q_{\text{cut}}^{l+1}) \left[ \tilde{\Pi}_{n+l}(t_c, \mu_Q^2; < Q_{\text{cut}}^{l+1}) O_{n+l} \right. \\ & \left. + \int_{t_c}^{\mu_Q^2} d\Phi_{+1} \frac{\tilde{D}_{n+l+1}}{B_{n+l}} \tilde{\Pi}_{n+l}(t, \mu_Q^2; < Q_{\text{cut}}^{l+1}) \Theta(Q_{\text{cut}}^{l+1} - Q_{n+l+1}) O_{n+l+1} \right] \\ & + \sum_{\{\tilde{f}\}} \int d\bar{\Phi}_{n+l+1} \tilde{H}_{n+l+1} \Theta(Q_{n+l} - Q_{\text{cut}}^l) \tilde{\Pi}_{n+l}(t_c, \mu_Q^2; > Q_{\text{cut}}^{l+1}) \Theta(Q_{\text{cut}}^{l+1} - Q_{n+l+1}) O_{n+l+1}. \end{aligned} \quad (4.20)$$

Like in the case of matching, the complete local cancellation of infrared singularities can only be guaranteed if the parton shower for the first step in the non-truncated evolution (below  $t_{n+l}$ ) contains full color and spin effects. If this is not the case, then a suppression factor must be implemented, damping the integrand in the single-soft region of gluon emission. However, a standard parton shower may be used for all emissions (or non-emissions) in the truncated shower, because soft and collinear singularities are regulated by the finite cutoff scales ( $t_{m+1}$  in Eqs. (4.18)).

Method	Shower Generator	Unitary	Accuracy	References
NL <sup>3</sup>	Ariadne/Pythia	No	NLO⊗PS	[89]
MEPS@NLO	Sherpa	No	NLO⊗PS	[87]
FxFx	Herwig(++)/Pythia	No	unknown	[90]
UNLOPS	Pythia	Yes	NLO⊗PS	[89, 91]

**Table 3:** Practically implemented NLO merging schemes.

If the definition of the jet measure,  $Q$ , and the evolution parameter of the parton shower,  $t$ , coincide, we can use this assumption to rewrite Eq. (4.20) as

$$\begin{aligned}
\langle O \rangle_l^{\text{excl}} &\rightarrow \int d\bar{\Phi}_{n+l} \tilde{B}_{n+l} \Theta(t_{n+l} - t_{\text{cut}}) \left( \prod_{i=n}^{n+l-1} \Pi_i^{(\text{PS})}(t_{i+1}, t_i) \right) \\
&\times \left[ \Pi_{n+l}(t_c, t_{n+l}) O_{n+l} + \int_{t_c}^{\mu_Q^2} d\Phi_{+1} \frac{\tilde{D}_{n+l+1}}{B_{n+l}} \Pi_{n+l}(t_{n+l+1}, t_{n+l}) \Theta(t_{\text{cut}} - t_{n+l+1}) O_{n+l+1} \right] \\
&+ \int d\bar{\Phi}_{n+l+1} \Theta(t_{n+l} - t_{\text{cut}}) H_{n+l+1} \left( \prod_{i=n}^{n+l} \Pi_i^{(\text{PS})}(t_{i+1}, t_i) \right) \Theta(t_{\text{cut}} - t_{n+l+1}) O_{n+l+1} .
\end{aligned} \tag{4.21}$$

We have indicated the potentially different nature of the no-branching probabilities for truncated showers using the superscript ( $PS$ ). We can now combine the subtraction terms in  $\tilde{B}_{n+l}$  and the no-branching probabilities on the first line. This makes the  $\mathcal{O}(\alpha_s)$  corrections to the leading-order merging formula, Eq. (4.17), explicit

$$\begin{aligned}
\langle O \rangle_l^{\text{excl}} &\rightarrow \int d\bar{\Phi}_{n+l} \Theta(t_{n+l} - t_{\text{cut}}) \tilde{B}_{n+l} \left[ \prod_{i=n}^{n+l-1} \Pi_i^{(\text{PS})}(t_{i+1}, t_i) \left( 1 + \frac{B_{n+l}}{B_{n+l}} \int_{t_{i+1}}^{t_i} d\Phi_{+1} \frac{D_{i+1}^{(\text{PS})}}{B_i} \right) \right] \\
&\times \left[ \Pi_{n+l}(t_c, t_{n+l}) O_{n+l} + \int_{t_c}^{\mu_Q^2} d\Phi_{+1} \frac{D_{n+l+1}}{B_{n+l}} \Pi_{n+l}(t_{n+l+1}, t_{n+l}) \Theta(t_{\text{cut}} - t_{n+l+1}) O_{n+l+1} \right] \\
&+ \int d\bar{\Phi}_{n+l+1} \Theta(t_{n+l} - t_{\text{cut}}) H_{n+l+1} \left( \prod_{i=n}^{n+l} \Pi_i^{(\text{PS})}(t_{i+1}, t_i) \right) \Theta(t_{\text{cut}} - t_{n+l+1}) O_{n+l+1} .
\end{aligned} \tag{4.22}$$

We have added arbitrary higher-order terms, which allow one to include the sum over truncated shower subtractions in the product of no-branching probabilities. Each term in the product can then be interpreted as the  $\mathcal{O}(\alpha_s)$ -subtracted, truncated, vetoed parton-shower no-branching probabilities for a particular final state. In practice, these expressions can be generated by running a truncated vetoed shower and skipping the first veto, depending on the ratio  $B_{n+l}/\tilde{B}_{n+l}$ . The remainder of the expression corresponds to an ordinary MC@NLO simulation, consisting of standard and hard remainder events, including the jet veto. This scheme is particularly easy to implement in practice, because no emissions need to be generated in the truncated shower.

There are several implementations of next-to-leading order merging methods at present. They differ in their theoretical accuracy and in the underlying parton-shower generator. They are listed in Tab. 3. An alternative scheme, based on known analytic resummed results combined with the parton shower also exists [92]. It allows to reach higher logarithmic accuracy for certain observables than attainable in the other methods.

Figure 7 shows a comparison between LO and NLO merged predictions for the jet multiplicity distribution in  $W$ -boson production at the Large Hadron Collider. The NLO prediction is given by the red histogram. Up to  $W+2$  jet final states are computed at NLO, and up to  $W+4$  jet final states are computed at LO. The theoretical uncertainty is given by the orange band. The LO prediction is given by the blue histogram, with the associated blue uncertainty band. Up to  $W+4$  jet matrix elements are included in this calculation.

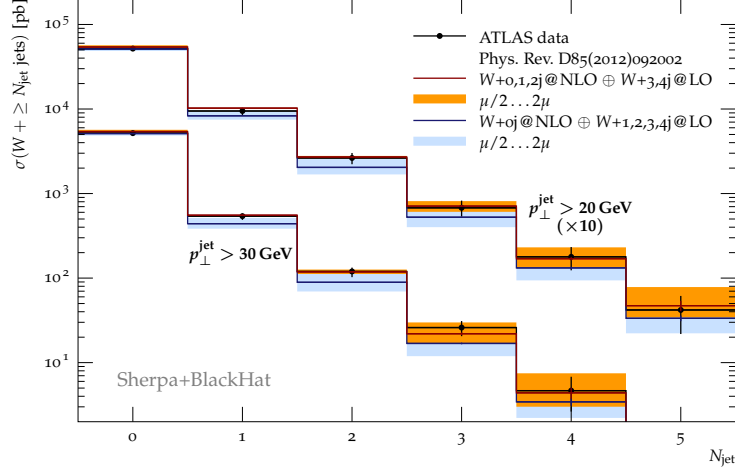


**Figure 7:** Comparison between LO and NLO merged results for  $W$ +jets production at the Large Hadron Collider. Figure taken from [93].

## 5 Underlying events

Up to this point we have relied on the strict factorization of the cross section for the production of a final state of large invariant mass or large invariant momentum transfer, Eq. (1.1). We have therefore neglected any effects of rescattering and the exchange of multiple partons between the initial-state protons. Such effects may, however, play a role in experiments. This can be anticipated by observing that the perturbative QCD cross section according to Eq. (1.1) is dominated by the exchange of  $t$ -channel gluons, which leads to a  $dp_T^2/p_T^4$  behavior of the partonic cross section, where  $p_T$  is the transverse momentum of the final-state parton. This behavior, which is shown in Fig. 8 leads to violations of the Froissart bound at high energies if the cutoff scale,  $p_{T,\min}$  is small enough.

The total cross section at hadron colliders consists of different components, which can be labeled according to the behavior of the beam particles after the scattering. If both beam particles survive the collision intact, the collision is called elastic. If one of them is excited, and the other stays intact, the collision is called single diffractive. If both are excited, with a large rapidity gap of no activity in between, the collision is called double diffractive. Finally, if both beam particles disintegrate and no rapidity gap is observed, the collision is called non-diffractive. The total hadronic cross section is then determined as the sum of all these contributions.

In this section we will focus only on the improved description of the non-diffractive part of the total cross section using multiple-parton scattering models. In very rough terms, this means that the non-diffractive cross section is saturated by more than a single partonic scattering, and that the number of partonic interactions is determined by a Poisson distribution. This model, which was originally proposed in [98] has been very successful in the description of many experimental measurements at hadron colliders.

The average multiplicity, according to the simple, impact-parameter independent model is given by

$$\langle n \rangle = \frac{\sigma_{\text{QCD}}(p_{\perp,\min}^2, s)}{\sigma_{\text{ND}}(s)}. \quad (5.1)$$

Assuming Poisson statistics, we can generate events in a Monte-Carlo simulation by defining a no-scattering probability that is equivalent to the no-branching probability in a parton shower:

$$\mathcal{P}_{\text{MPI}}(p_T, \mu_{\text{MPI}}^2) = \exp \left\{ - \frac{1}{\sigma_{\text{ND}}} \int_{p_T}^{\mu_{\text{MPI}}^2} d\bar{p}_T^2 \frac{d\sigma_{\text{QCD}}}{d\bar{p}_T^2} \right\}. \quad (5.2)$$

Events can then be generated using the veto algorithm in Sec. 3.2. It is interesting to observe that the functional form of the hard QCD cross section is maintained by this formalism, due to the properties

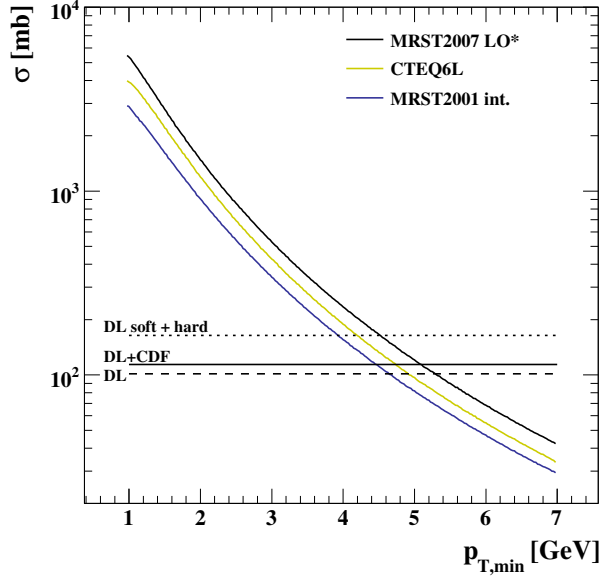


**Figure 8:** The inclusive jet cross section at LO for different PDF sets, compared to various extrapolations of non-perturbative fits to the total proton-proton cross section at 14 TeV. The dashed line gives the prediction based on a parametrization by Donnachie and Landshoff [94], the solid line stems from the same fit, but constrained by CDF data [95]. The dotted line is predicted by the most recent fit [96], which includes contributions from both hard and soft Pomerons. Figure taken from [97].

of Poisson distributions. The total probability for any  $2 \rightarrow 2$  QCD scattering in this model to occur at hardness scale  $p_T$  is given by precisely the integrand in the exponent of Eq. (5.2).

The event structure in hadronic interactions may actually be very complex, leading to situations where a single initial-state parton can split into two before both of them enter a hard collision. At the same time an independently resolved parton may undergo another collision, while all of them collectively radiate further gluons. Clearly, this situation is too complex to be described exactly. But a good fraction of it may be modeled in event generators with an interleaved initial-state parton shower and multiple interaction evolution [71]. The combined no-branching probability for such an evolution is given by

$$\mathcal{P}_{\text{MPI+PS}}(p_T) = \mathcal{P}_{\text{MPI}}(p_T) \Pi(p_T), \quad (5.3)$$

where  $\Pi(p_T)$  is the no-branching probability of the parton shower, Eq. (3.8). Multiple interaction evolution and parton-shower evolution must have a common evolution variable for this model to be applicable. A possible resulting event structure, together with the associated scales at which the partons are resolved is depicted Fig. 9.

The structure of beam remnants and their connection with the many hard and semi-hard scatterings, especially the treatment of baryon number, is intricate once multiple parton interactions are included in the Monte-Carlo simulation. In simulations without a hard underlying event, baryon number is normally carried by the diquark remnant of the proton. This model must be improved when multiple scatterings are included [99].

It is also necessary to consider the finite size of hadrons. Each proton-proton collision can be characterized by an impact parameter  $b$ , which measures the transverse separation of the centers of incoming hadrons in position space. If  $\rho(\mathbf{x})$  denotes the (suitably Lorentz contracted) hadronic-matter distribution, the time-integrated overlap between the two distributions in the center of mass frame is given by

$$\tilde{O}(b) = \int d^3\mathbf{x} dt \rho_{1b} \left( x - \frac{1}{2} b, y, z - vt \right) \rho_{2b} \left( x + \frac{1}{2} b, y, z + vt \right) \quad (5.4)$$

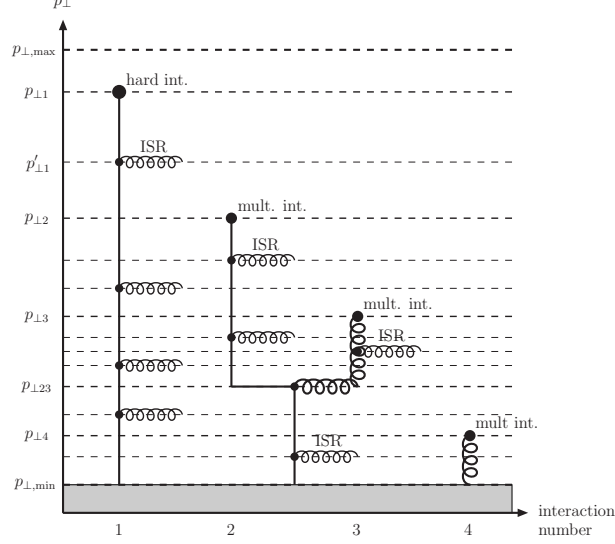


**Figure 9:** Sketch of interleaved parton shower and multiple scattering evolution. The evolution proceeds in the negative  $p_{\perp}$  direction. The hard scattering takes place at  $p_{\perp,1}$ , followed by parton-shower emissions. The first secondary scattering happens at  $p_{\perp,2}$ . At  $p_{T,23}$ , two parton-shower initiators are generated by splitting of a single initial-state parton. Figure taken from [71].

It is natural to assume that there is a linear relationship between the overlap and the mean number of hard interactions in the event,  $\langle \tilde{n}(b) \rangle = k \tilde{O}(b)$ . However, we also have the requirement that each event contain at least one hard interaction. For each impact parameter the number of interactions should be Poisson distributed. This requires that

$$\langle \tilde{n}(b) \rangle = \frac{k \tilde{O}(b)}{1 - \exp\{-k \tilde{O}(b)\}} = \frac{k \tilde{O}(b)}{P_{\text{int}}(b)} . \quad (5.5)$$

with  $P_{\text{int}}(b) = 1 - \exp\{-k \tilde{O}(b)\}$  the total interaction probability. When averaged over all impact parameters,  $\langle n(b) \rangle$  must satisfy Eq. (5.1), requiring that:

$$\frac{\sigma_{\text{QCD}}(p_{T,\text{min}}, s)}{\sigma_{\text{ND}}(s)} = \frac{\int_0^\infty d^2\mathbf{b} k \tilde{O}(b)}{\int_0^\infty d^2\mathbf{b} P_{\text{int}}(b)} . \quad (5.6)$$

This allows one to compute the constant of proportionality,  $k$ . As the normalization of  $\tilde{O}(b)$  is irrelevant, it is convenient to introduce an enhancement factor  $f(b)$ , gauging how the interaction probability for a given impact parameter  $b$  compares to the suitably defined average [98]

$$\langle \tilde{n}(b) \rangle = f(b) \langle k \tilde{O} \rangle . \quad (5.7)$$

This enhancement factor is normalized such that  $\langle f \rangle = 1$ . The average number of scatterings  $\langle \tilde{n}(b) \rangle$  is

$$\langle \tilde{n}(b) \rangle = f_c f(b) \frac{\sigma_{\text{QCD}}(p_{T,\text{min}}, s)}{\sigma_{\text{ND}}(s)} . \quad (5.8)$$

The full no-scattering probability in this model is the given as

$$\mathcal{P}_{\text{MPI}}(b, p_T, \mu_{\text{MPI}}^2) = \exp \left\{ -f_c f(b) \frac{1}{\sigma_{\text{ND}}} \int_{p_T}^{\mu_{\text{MPI}}^2} d\bar{p}_T^2 \frac{d\sigma_{\text{QCD}}}{d\bar{p}_T^2} \right\} . \quad (5.9)$$

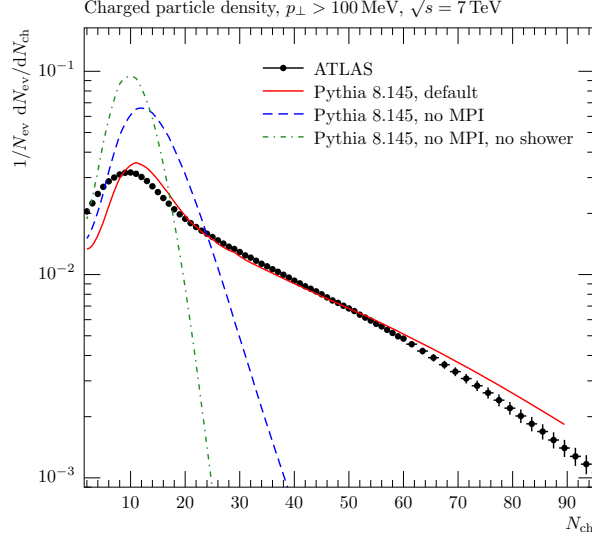


**Figure 10:** Effects of the simulation of Multiple Parton Scatterings (MPI) on the charged particle multiplicity distribution at the LHC as measured by the ATLAS experiment [100]. Figure taken from [2].

One can assume different hadronic matter distributions, like exponential, Gaussian or double Gaussian distributions. More complicated pictures can also be imagined.

It may also be useful to model saturation effects by requiring a hard cross section which has no sharp cutoff at the minimum scale  $p_{T,\min}$ . The simplest possible procedure to account for this effect is to regularize the differential cross section by including a factor

$$\frac{p_T^4}{(p_T^2 + p_{T0}^2)^2} \frac{\alpha_s^2(p_T^2 + p_{T0}^2)}{\alpha_s^2(p_T^2)}, \quad (5.10)$$

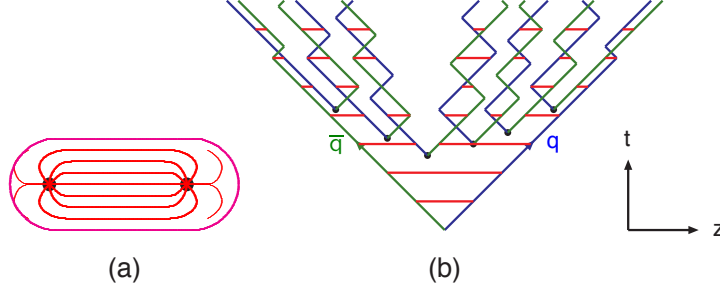
where  $p_{T0}$  is the regularization scale.

Figure 10 shows the effect of the simulation of multiple scattering effects on the prediction for the charged particle multiplicity spectra at the Large Hadron Collider. It is evident that without a simulation of multiple interactions, the data cannot be described properly.

Since the original proposal for the simulation of multiple interactions [98], a variety of other models have been implemented in general-purpose event generators [71, 101, 102]. A review of the related models and predictions is given in [2]. Other, more inclusive approaches to hadron-hadron scattering, which naturally include multiple scattering effects also exist [103, 104].

## 6 Hadronization

To complete the simulation of realistic event topologies as observable experimentally, the quarks and gluons from hard scattering simulations, parton showers and multiple scattering simulations must be transformed into color-neutral final states. In the context of a Monte-Carlo simulation this process is called hadronization or jet fragmentation. Traditionally, the first hadronization model applicable to Monte-Carlo simulation was the Feynman-Field model [105]. It gives a recipe to produce mesons iteratively starting from a single quark. Because the hadronization of each parton is considered separately in this model, it is also called “independent fragmentation”. However, it suffers from frame dependence and collinear unsafety. The two hadronization models used today are the string and cluster models, which are based on the ideas pioneered in [106].



**Figure 11:** Left: Flux tube spanned between quark and antiquark. Right: Motion and breakup of a string system in the longitudinal direction over time. Figure taken from [2].

## 6.1 String model

The string or Lund model of jet fragmentation [107, 108] is based on the observation that the quark-antiquark potential rises linearly with the distance between quarks in a meson system. This effect is measurable in quarkonium spectra, and it has been computed using lattice QCD in the quenched approximation [109]. It translates into a physical picture where a flux tube is stretched between the two quarks, with constant energy per unit length, leading to a potential  $V(r) = \kappa r$  where  $\kappa \approx 1 \text{ GeV/fm}$ . A sketch of such a flux tube is shown in Fig. 11 (left).

A Lorentz covariant and causal description of the energy flow in the flux tube is obtained by the dynamics of a massless relativistic string with no transverse degrees of freedom, which parametrizes the longitudinal axis of the flux tube. As a quark-antiquark pair produced at high energy moves apart at the speed of light, the potential energy stored in the string stretched between it can lead to the creation of a new quark-antiquark pair, such that the system splits into two color-neutral strings with a quark/antiquark at either end. If the energy stored the field between the new quark-antiquark pairs is large enough, further string breaks may occur until no further partitioning is possible and the quarks enter into “yo-yo” motion about each other. This is shown in Fig. 11 (right). The space-time picture can be mapped onto a corresponding picture in momentum space, where  $dp_z/dt = \kappa$ . Different string breaks are causally separated. The fragmentation function describing the string breakup should therefore exhibit left-right symmetry.

The Lund model proposes the use of the Lund symmetric fragmentation function,

$$f(z) \propto \frac{1}{z} (1-z)^\alpha \exp\left(-\frac{b m_T^2}{z}\right). \quad (6.1)$$

where  $z$  is the remaining light-cone momentum fraction of the quark (antiquark) in the  $+z$  ( $-z$ ) direction and  $a$  and  $b$  are free parameters [110]. A slightly modified form is introduced for heavy quarks [111]. The transverse motion of the newly-created quarks/antiquarks is parametrized as a quantum mechanical tunneling effect, with probability proportional to

$$\exp\left(-\frac{\pi m_T^2}{\kappa}\right) = \exp\left(-\frac{\pi m^2}{\kappa}\right) \exp\left(-\frac{\pi p_T^2}{\kappa}\right) \quad (6.2)$$

The factorization of mass and transverse momentum dependence then leads to a flavor-independent transverse-momentum spectra of the hadrons with an average of  $\langle p_T^2 \rangle = 2\kappa/\pi$ . Equation (6.2) also implies a natural heavy-flavor suppression.

In the simplest scheme for baryon production, diquark pairs are produced instead of quark pairs. A more advanced model is the popcorn approach, where baryons appear from multiple production of quark pairs. Gluons are accommodated in the string model as kinks on the flux tube stretched between the two initial quarks. As such, the gluon can also be assigned the incoherent sum of a color and an anticolor charge, which effectively models the dynamics of the color field in the large- $N_C$  approximation (cf.



### Primary Light Clusters

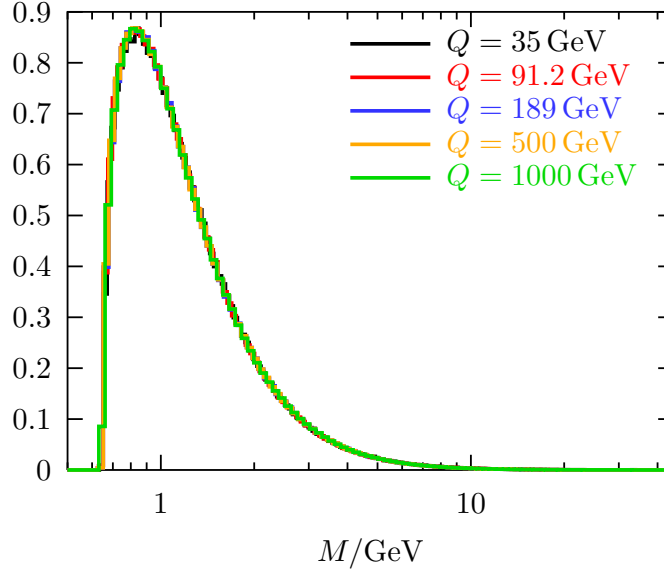


**Figure 12:** Invariant mass distribution of color singlet clusters in the cluster model. Figure taken from [2].

Sec. 3.4). This leads to a genuine prediction of the Lund string model, called the string effect: Final states containing a quark-antiquark pair and a gluon should receive enhanced hadron production in the angular regions between the quark and the gluon and the gluon and the antiquark. This was confirmed in experiments [112]. Crucially, the string model of jet fragmentation is infrared and collinear safe, because a soft or collinear gluon induces a vanishingly small kink on the color string [113].

Pythia [49, 114] is the only Monte-Carlo event generator which currently implements the string model.

## 6.2 Cluster model

The cluster-hadronization model is based on the so-called preconfinement property of QCD [115]. This means that at each point the parton shower forms color-singlet combinations of partons, called clusters, which have an asymptotically universal invariant mass distribution. In this context, universal means that the distribution only depends on the cutoff scale  $t_c$  of the parton shower and on  $\Lambda_{\text{QCD}}$ , but not on the center-of-mass energy of the collision [115, 116]. This is shown in Fig. 12 for a variety of center-of-mass energies in  $e^+e^-$  collisions.

Preconfinement can be inferred from the topology of parton-shower final states, where color-adjacent partons, due to the large- $N_C$  approximation, are also adjacent in phase space, as adjacency implies they likely originated at the same evolution scale. Therefore clusters of large invariant mass are suppressed.

The first hadronization model based on preconfinement was the Field-Fox-Wolfram model [117, 118]. In this model, a non-perturbative splitting of final-state gluons into quarks is enforced at the end of the parton-shower evolution. Adjacent color lines then form primary clusters with a mass distribution as shown in Fig. 12. The mass distribution of these final states is closely connected to hadron spectra, an effect known as local parton-hadron duality [119, 120]. The flavor assignment in gluon splitting is important to obtain the correct heavy flavor suppression. This can be approximated to a good extent by kinematic effects, which reduce the phase space for heavy flavor production.

Once primary clusters are formed, the ones with mass below 3-4 GeV are transformed into hadrons through a two-body decay according to phase space. Heavier clusters may first undergo non-perturbative splitting processes, and decay into two lighter clusters, or a lighter cluster and a hadron, before the

cluster-to-hadron transition is resumed. This process is repeated until all clusters have been transformed into hadrons. Very low mass clusters may transition directly into hadrons, in which case another hadron or cluster must absorb the recoil if the cluster mass is different from the hadron mass.

Two cluster-hadronization models are currently widely used, which are implemented in Herwig++ [121] and Sherpa [122].

## 7 Summary

Parton-shower event generators are indispensable tools for particle physics phenomenology at hadron colliders. They are used in the planning of new experiments, detector design and performance studies, and in the extraction of theoretical parameters from the measurements themselves.

Event simulation in modern generators starts with the computation of hard interactions, often at higher orders in perturbation theory. QCD Bremsstrahlung is then simulated using the parton-shower approach, and the resummed higher-order calculation of the parton shower is matched to / merged with the higher-order fixed-order calculations for the hard processes. Multiple scattering effects are simulated by repeated generation of hard processes according to the hard cross sections for jet production in perturbative QCD, such that the non-diffractive part of the total cross section is saturated. Eventually, the perturbatively-computed final state is transformed into measurable hadrons by means of hadronization models.

Event generators traditionally contain several free parameters, especially in the simulation of hadronization and multiple scattering effects. The simulation of hard QCD radiation, however, is based on perturbative QCD in the parton shower approximation, which is to a large extent defined by the factorization properties of QCD amplitudes and color-coherence effects in soft gluon emission.

## Acknowledgments

I wish to thank the scientific organizers of TASI 2014, Lance Dixon and Frank Petriello, and the local organizers, Tom Degrand and Kalyana Mahanthappa for a great school, and for the enjoyable time together at UC Boulder. Many thanks to Valentin Hirschi for his help in organizing and running the Monte-Carlo tutorials and to all the students for interesting discussions and a great atmosphere during the lectures and tutorials. This work was supported by the US Department of Energy under contract DE-AC02-76SF00515.

## References

- [1] B. Webber, *Monte Carlo Simulation of Hard Hadronic Processes*, Ann. Rev. Nucl. Part. Sci. **36** (1986), 253–286.
- [2] A. Buckley et al., *General-purpose event generators for LHC physics*, Phys. Rept. **504** (2011), 145–233, [[arXiv:1101.2599](#) [hep-ph]].
- [3] G. T. Bodwin, *Factorization of the Drell-Yan Cross-Section in Perturbation Theory*, Phys.Rev. **D31** (1985), 2616.
- [4] J. C. Collins, D. E. Soper and G. F. Sterman, *Factorization for Short Distance Hadron - Hadron Scattering*, Nucl.Phys. **B261** (1985), 104.
- [5] J. C. Collins, D. E. Soper and G. Sterman, *Soft gluons and factorization*, Nucl. Phys. **B308** (1988), 833–856.
- [6] L. J. Dixon, *Calculating scattering amplitudes efficiently*, [hep-ph/9601359](#).
- [7] L. J. Dixon, *A brief introduction to modern amplitude methods*, [arXiv:1310.5353](#) [hep-ph].

- [8] V. N. Gribov and L. N. Lipatov, *Deep inelastic e-p scattering in perturbation theory*, Sov. J. Nucl. Phys. **15** (1972), 438–450.
- [9] L. N. Lipatov, *The parton model and perturbation theory*, Sov. J. Nucl. Phys. **20** (1975), 94–102.
- [10] Y. L. Dokshitzer, *Calculation of the structure functions for deep inelastic scattering and  $e^+e^-$  annihilation by perturbation theory in quantum chromodynamics*, Sov. Phys. JETP **46** (1977), 641–653.
- [11] G. Altarelli and G. Parisi, *Asymptotic freedom in parton language*, Nucl. Phys. **B126** (1977), 298–318.
- [12] V. V. Sudakov, *Vertex parts at very high-energies in quantum electrodynamics*, Sov. Phys. JETP **3** (1956), 65–71.
- [13] S. Catani and M. H. Seymour, *A general algorithm for calculating jet cross sections in NLO QCD*, Nucl. Phys. **B485** (1997), 291–419, [[hep-ph/9605323](#)].
- [14] G. P. Salam, *Towards jetography*, Eur. Phys. J. **C67** (2010), 637–686, [[arXiv:0906.1833 \[hep-ph\]](#)].
- [15] S. Plätzer and M. Sjödal, *Subleading  $N_c$  improved Parton Showers*, JHEP **07** (2012), 042, [[arXiv:1201.0260 \[hep-ph\]](#)].
- [16] M. L. Mangano, S. J. Parke and Z. Xu, *Duality and multi-gluon scattering*, Nucl. Phys. **B298** (1988), 653.
- [17] A. Kanaki and C. G. Papadopoulos, *HELAC: A package to compute electroweak helicity amplitudes*, Comput. Phys. Commun. **132** (2000), 306–315, [[hep-ph/0002082](#)].
- [18] F. Maltoni, K. Paul, T. Stelzer and S. Willenbrock, *Color-flow decomposition of QCD amplitudes*, Phys. Rev. **D67** (2003), 014026, [[hep-ph/0209271](#)].
- [19] V. del Duca, A. Frizzo and F. Maltoni, *Factorization of tree QCD amplitudes in the high-energy limit and in the collinear limit*, Nucl. Phys. **B568** (2000), 211–262, [[hep-ph/9909464](#)].
- [20] V. Del Duca, L. J. Dixon and F. Maltoni, *New color decompositions for gauge amplitudes at tree and loop level*, Nucl. Phys. **B571** (2000), 51–70, [[hep-ph/9910563](#)].
- [21] H. Weyl, *The Theory of Groups and Quantum Mechanics*, Dover, New York, USA, 1931.
- [22] B. L. van der Waerden, *Group Theory and Quantum Mechanics*, Springer, Berlin, Germany, 1974, Die Grundlehren der math. Wissenschaften.
- [23] S. Dittmaier, *Weyl-van der Waerden formalism for helicity amplitudes of massive particles*, Phys. Rev. **D59** (1999), 016007, [[hep-ph/9805445](#)].
- [24] K. Hagiwara and D. Zeppenfeld, *Helicity amplitudes for heavy lepton production in  $e^+e^-$  annihilation*, Nucl. Phys. **B274** (1986), 1.
- [25] F. A. Berends and W. T. Giele, *Recursive calculations for processes with  $n$  gluons*, Nucl. Phys. **B306** (1988), 759.
- [26] A. Cafarella, C. G. Papadopoulos and M. Worek, *Helac-Phegas: A generator for all parton level processes*, Comput. Phys. Commun. **180** (2009), 1941–1955, [[arXiv:0710.2427 \[hep-ph\]](#)].
- [27] E. Byckling and K. Kajantie,  *$N$ -particle phase space in terms of invariant momentum transfers*, Nucl. Phys. **B9** (1969), 568–576.
- [28] R. Kleiss and R. Pittau, *Weight optimization in multichannel Monte Carlo*, Comput. Phys. Commun. **83** (1994), 141–146, [[hep-ph/9405257](#)].
- [29] F. James, *Monte-Carlo phase space*, CERN-68-15.

- [30] G. P. Lepage, *VEGAS - An Adaptive Multi-dimensional Integration Program*, CLNS-80/447.
- [31] T. Ohl, *Vegas revisited: Adaptive Monte Carlo integration beyond factorization*, Comput. Phys. Commun. **120** (1999), 13–19, [[hep-ph/9806432](#)].
- [32] S. Jadach, *Foam: Multi-dimensional general purpose Monte Carlo generator with self-adapting simplicial grid*, Comput. Phys. Commun. **130** (2000), 244–259, [[physics/9910004](#)].
- [33] S. Frixione, Z. Kunszt and A. Signer, *Three-jet cross-sections to next-to-leading order*, Nucl. Phys. **B467** (1996), 399–442, [[hep-ph/9512328](#)].
- [34] S. Catani, S. Dittmaier, M. H. Seymour and Z. Trocsanyi, *The dipole formalism for next-to-leading order QCD calculations with massive partons*, Nucl. Phys. **B627** (2002), 189–265, [[hep-ph/0201036](#)].
- [35] T. Binoth et al., *A proposal for a standard interface between Monte Carlo tools and one-loop programs*, Comput. Phys. Commun. **181** (2010), 1612–1622, [[arXiv:1001.1307](#) [hep-ph]].
- [36] S. Alioli et al., *Update of the Binoth Les Houches Accord for a standard interface between Monte Carlo tools and one-loop programs*, Comput.Phys.Commun. **185** (2014), 560–571, [[arXiv:1308.3462](#) [hep-ph]].
- [37] S. Frixione and B. R. Webber, *Matching NLO QCD computations and parton shower simulations*, JHEP **06** (2002), 029, [[hep-ph/0204244](#)].
- [38] P. Nason, *A new method for combining NLO QCD with shower Monte Carlo algorithms*, JHEP **11** (2004), 040, [[hep-ph/0409146](#)].
- [39] S. Frixione, P. Nason and C. Oleari, *Matching NLO QCD computations with parton shower simulations: the POWHEG method*, JHEP **11** (2007), 070, [[arXiv:0709.2092](#) [hep-ph]].
- [40] F. Bloch and A. Nordsieck, *Note on the Radiation Field of the electron*, Phys. Rev. **52** (1937), 54–59.
- [41] T. Kinoshita, *Mass Singularities of Feynman Amplitudes*, J.Math.Phys. **3** (1962), 650–677.
- [42] T. Lee and M. Nauenberg, *Degenerate Systems and Mass Singularities*, Phys. Rev. **133** (1964), B1549–B1562.
- [43] A. Bassetto, M. Ciafaloni and G. Marchesini, *Jet structure and infrared sensitive quantities in perturbative QCD*, Phys. Rept. **100** (1983), 201–272.
- [44] S. Frixione, *A general approach to jet cross sections in QCD*, Nucl. Phys. **B507** (1997), 295–314, [[hep-ph/9706545](#)].
- [45] T. Gleisberg and F. Krauss, *Automating dipole subtraction for QCD NLO calculations*, Eur. Phys. J. **C53** (2008), 501–523, [[arXiv:0709.2881](#) [hep-ph]].
- [46] M. Czakon, C. Papadopoulos and M. Worek, *Polarizing the dipoles*, JHEP **08** (2009), 085, [[arXiv:0905.0883](#) [hep-ph]].
- [47] R. Frederix, T. Gehrmann and N. Greiner, *Automation of the Dipole Subtraction Method in MadGraph/MadEvent*, JHEP **09** (2008), 122, [[arXiv:0808.2128](#) [hep-ph]].
- [48] R. Frederix, T. Gehrmann and N. Greiner, *Integrated dipoles with MadDipole in the MadGraph framework*, JHEP **06** (2010), 086, [[arXiv:1004.2905](#) [hep-ph]].
- [49] T. Sjöstrand, S. Mrenna and P. Skands, *PYTHIA 6.4 physics and manual*, JHEP **05** (2006), 026, [[hep-ph/0603175](#)].
- [50] R. K. Ellis, W. J. Stirling and B. R. Webber, *QCD and collider physics*, ed. 1, vol. 8, Cambridge Monogr. Part. Phys. Nucl. Phys. Cosmol., 1996.

- [51] H. Kharraziha and L. Lönnblad, *The linked dipole chain Monte Carlo*, JHEP **03** (1998), 006, [[hep-ph/9709424](#)].
- [52] Z. Nagy and D. E. Soper, *Parton showers with quantum interference*, JHEP **09** (2007), 114, [[arXiv:0706.0017](#) [hep-ph]].
- [53] S. Höche, F. Krauss, M. Schönherr and F. Siegert, *A critical appraisal of NLO+PS matching methods*, JHEP **09** (2012), 049, [[arXiv:1111.1220](#) [hep-ph]].
- [54] L. Lönnblad, *Fooling Around with the Sudakov Veto Algorithm*, Eur.Phys.J. **C73** (2013), 2350, [[arXiv:1211.7204](#) [hep-ph]].
- [55] Y. L. Dokshitzer, D. Diakonov and S. Troian, *Inelastic processes in Quantum Chromodynamics*, SLAC-TRANS-0183.
- [56] D. Amati, R. Petronzio and G. Veneziano, *Relating hard QCD processes through universality of mass singularities. 2*, Nucl. Phys. **B146** (1978), 29–49.
- [57] R. K. Ellis, H. Georgi, M. Machacek, H. D. Politzer and G. G. Ross, *Factorization and the Parton Model in QCD*, Phys.Lett. **B78** (1978), 281.
- [58] S. B. Libby and G. F. Sterman, *High-energy Behavior of Jet and Lepton Pair Production*, Phys.Lett. **B78** (1978), 618–622.
- [59] A. H. Mueller, *Cut Vertices and their Renormalization: A Generalization of the Wilson Expansion*, Phys.Rev. **D18** (1978), 3705.
- [60] Y. L. Dokshitzer, D. Diakonov and S. I. Troian, *Hard Processes in Quantum Chromodynamics*, Phys. Rept. **58** (1980), 269–395.
- [61] S. Catani, B. R. Webber and G. Marchesini, *QCD coherent branching and semiinclusive processes at large  $x$* , Nucl. Phys. **B349** (1991), 635–654.
- [62] G. Gustafson and U. Pettersson, *Dipole formulation of QCD cascades*, Nucl. Phys. **B306** (1988), 746.
- [63] L. Lönnblad, *Ariadne version 4: A program for simulation of QCD cascades implementing the colour dipole model*, Comput. Phys. Commun. **71** (1992), 15–31.
- [64] S. Höche and S. Prestel, *The midpoint between dipole and parton showers*, [arXiv:1506.05057](#) [hep-ph].
- [65] G. Marchesini and B. R. Webber, *Monte Carlo Simulation of General Hard Processes with Coherent QCD Radiation*, Nucl. Phys. **B310** (1988), 461.
- [66] G. Corcella et al., *HERWIG 6: an event generator for hadron emission reactions with interfering gluons (including supersymmetric processes)*, JHEP **01** (2001), 010, [[hep-ph/0011363](#)].
- [67] S. Gieseke, P. Stephens and B. Webber, *New formalism for QCD parton showers*, JHEP **12** (2003), 045, [[hep-ph/0310083](#)].
- [68] S. Plätzer and S. Gieseke, *Coherent Parton Showers with Local Recoils*, JHEP **01** (2011), 024, [[arXiv:0909.5593](#) [hep-ph]].
- [69] T. Sjöstrand, *A model for initial state parton showers*, Phys. Lett. **B157** (1985), 321.
- [70] M. Bengtsson and T. Sjöstrand, *A comparative study of coherent and non-coherent parton shower evolution*, Nucl. Phys. **B289** (1987), 810.
- [71] T. Sjöstrand and P. Z. Skands, *Transverse-momentum-ordered showers and interleaved multiple interactions*, Eur. Phys. J. **C39** (2005), 129–154, [[hep-ph/0408302](#)].

- [72] R. Kuhn, F. Krauss, B. Ivanyi and G. Soff, *APACIC++ 1.0: A PArton Cascade In C++*, Comput. Phys. Commun. **134** (2001), 223–266, [[hep-ph/0004270](#)].
- [73] S. Schumann and F. Krauss, *A parton shower algorithm based on Catani-Seymour dipole factorisation*, JHEP **03** (2008), 038, [[arXiv:0709.1027](#) [hep-ph]].
- [74] W. T. Giele, D. A. Kosower and P. Z. Skands, *A Simple shower and matching algorithm*, Phys. Rev. **D78** (2008), 014026, [[arXiv:0707.3652](#) [hep-ph]].
- [75] W. T. Giele, D. A. Kosower and P. Z. Skands, *Higher-Order Corrections to Timelike Jets*, Phys. Rev. **D84** (2011), 054003, [[arXiv:1102.2126](#) [hep-ph]].
- [76] P. Nason and B. Webber, *Next-to-Leading-Order Event Generators*, Ann.Rev.Nucl.Part.Sci. **62** (2012), 187–213, [[arXiv:1202.1251](#) [hep-ph]].
- [77] S. Alioli, P. Nason, C. Oleari and E. Re, *NLO vector-boson production matched with shower in POWHEG*, JHEP **07** (2008), 060, [[arXiv:0805.4802](#) [hep-ph]].
- [78] S. Alioli, P. Nason, C. Oleari and E. Re, *NLO Higgs boson production via gluon fusion matched with shower in POWHEG*, JHEP **04** (2009), 002, [[arXiv:0812.0578](#) [hep-ph]].
- [79] L. Lönnblad, *Correcting the colour-dipole cascade model with fixed order matrix elements*, JHEP **05** (2002), 046, [[hep-ph/0112284](#)].
- [80] L. Lönnblad and S. Prestel, *Unitarising Matrix Element + Parton Shower merging*, JHEP **02** (2013), 094, [[arXiv:1211.4827](#) [hep-ph]].
- [81] S. Plätzer, *Controlling inclusive cross sections in parton shower + matrix element merging*, JHEP **08** (2013), 114, [[arXiv:1211.5467](#) [hep-ph]].
- [82] M. L. Mangano, M. Moretti and R. Pittau, *Multijet matrix elements and shower evolution in hadronic collisions:  $Wb\bar{b} + n$ -jets as a case study*, Nucl. Phys. **B632** (2002), 343–362, [[hep-ph/0108069](#)].
- [83] J. Alwall et al., *Comparative study of various algorithms for the merging of parton showers and matrix elements in hadronic collisions*, Eur. Phys. J. **C53** (2008), 473–500, [[arXiv:0706.2569](#) [hep-ph]].
- [84] S. Catani, F. Krauss, R. Kuhn and B. R. Webber, *QCD matrix elements + parton showers*, JHEP **11** (2001), 063, [[hep-ph/0109231](#)].
- [85] F. Krauss, *Matrix elements and parton showers in hadronic interactions*, JHEP **08** (2002), 015, [[hep-ph/0205283](#)].
- [86] L. Lönnblad and S. Prestel, *Matching Tree-Level Matrix Elements with Interleaved Showers*, JHEP **03** (2012), 019, [[arXiv:1109.4829](#) [hep-ph]].
- [87] S. Höche, F. Krauss, S. Schumann and F. Siegert, *QCD matrix elements and truncated showers*, JHEP **05** (2009), 053, [[arXiv:0903.1219](#) [hep-ph]].
- [88] K. Hamilton, P. Richardson and J. Tully, *A modified CKKW matrix element merging approach to angular-ordered parton showers*, JHEP **11** (2009), 038, [[arXiv:0905.3072](#) [hep-ph]].
- [89] N. Lavesson and L. Lönnblad, *Extending CKKW-merging to one-loop matrix elements*, JHEP **12** (2008), 070, [[arXiv:0811.2912](#) [hep-ph]].
- [90] R. Frederix and S. Frixione, *Merging meets matching in MC@NLO*, JHEP **12** (2012), 061, [[arXiv:1209.6215](#) [hep-ph]].
- [91] L. Lönnblad and S. Prestel, *Merging Multi-leg NLO Matrix Elements with Parton Showers*, JHEP **03** (2013), 166, [[arXiv:1211.7278](#) [hep-ph]].

- [92] S. Alioli, C. W. Bauer, C. J. Berggren, A. Hornig, F. J. Tackmann et al., *Combining Higher-Order Resummation with Multiple NLO Calculations and Parton Showers in GENEVA*, JHEP **09** (2013), 120, [[arXiv:1211.7049](#) [hep-ph]].
- [93] S. Höche, F. Krauss, M. Schönherr and F. Siegert, *QCD matrix elements + parton showers: The NLO case*, JHEP **04** (2013), 027, [[arXiv:1207.5030](#) [hep-ph]].
- [94] A. Donnachie and P. V. Landshoff, *Total cross sections*, Phys. Lett. **B296** (1992), 227–232, [[hep-ph/9209205](#)].
- [95] F. Abe et al., The CDF collaboration, *Measurement of the  $\bar{p}p$  total cross-section at  $\sqrt{s} = 546$  GeV and 1800-GeV*, Phys.Rev. **D50** (1994), 5550–5561.
- [96] A. Donnachie and P. Landshoff, *Does the hard pomeron obey Regge factorization?*, Phys.Lett. **B595** (2004), 393–399, [[arXiv:hep-ph/0402081](#) [hep-ph]].
- [97] M. Bähr, J. M. Butterworth and M. H. Seymour, *The Underlying Event and the Total Cross Section from Tevatron to the LHC*, JHEP **01** (2009), 065, [[arXiv:0806.2949](#) [hep-ph]].
- [98] T. Sjöstrand and M. van Zijl, *A multiple-interaction model for the event structure in hadron collisions*, Phys. Rev. **D36** (1987), 2019.
- [99] T. Sjöstrand and P. Z. Skands, *Multiple interactions and the structure of beam remnants*, JHEP **03** (2004), 053, [[hep-ph/0402078](#)].
- [100] G. Aad et al., The ATLAS Collaboration collaboration, *Charged-particle multiplicities in pp interactions measured with the ATLAS detector at the LHC*, New J.Phys. **13** (2011), 053033, [[arXiv:1012.5104](#) [hep-ex]].
- [101] J. M. Butterworth, J. R. Forshaw and M. H. Seymour, *Multiparton Interactions in Photoproduction at HERA*, Z. Phys. **C72** (1996), 637–646, [[hep-ph/9601371](#)].
- [102] M. Bähr, S. Gieseke and M. H. Seymour, *Simulation of multiple partonic interactions in Herwig++*, JHEP **07** (2008), 076, [[arXiv:0803.3633](#) [hep-ph]].
- [103] C. Flensburg, G. Gustafson and L. Lönnblad, *Inclusive and Exclusive observables from dipoles in high energy collisions*, JHEP **08** (2011), 103, [[arXiv:1103.4321](#) [hep-ph]].
- [104] A. Martin, H. Hoeth, V. Khoze, F. Krauss, M. Ryskin et al., *Diffraction Physics*, PoS **QNP2012** (2012), 017, [[arXiv:1206.2124](#) [hep-ph]].
- [105] R. D. Field and R. P. Feynman, *A parametrization of the properties of quark jets*, Nucl. Phys. **B136** (1978), 1.
- [106] X. Artru and G. Mennessier, *String model and multiproduction*, Nucl. Phys. **B70** (1974), 93–115.
- [107] B. Andersson, G. Gustafson, G. Ingelman and T. Sjöstrand, *Parton Fragmentation and String Dynamics*, Phys. Rept. **97** (1983), 31–145.
- [108] B. Andersson, *The Lund model*, vol. 7, Camb. Monogr. Part. Phys. Nucl. Phys. Cosmol., 1997.
- [109] G. Bali and K. Schilling, *Static quark - anti-quark potential: Scaling behavior and finite size effects in SU(3) lattice gauge theory*, Phys.Rev. **D46** (1992), 2636–2646.
- [110] B. Andersson, G. Gustafson and B. Söderberg, *A general model for jet fragmentation*, Z. Phys. **C20** (1983), 317.
- [111] M. G. Bowler,  *$e^+e^-$  production of heavy quarks in the string model*, Z. Phys. **C11** (1981), 169.
- [112] W. Bartel et al., The JADE Collaboration collaboration, *Particle Distribution in Three Jet Events Produced by  $e^+e^-$  Annihilation*, Z.Phys. **C21** (1983), 37.

- [113] T. Sjöstrand, *Jet Fragmentation of Nearby Partons*, Nucl.Phys. **B248** (1984), 469.
- [114] T. Sjöstrand, S. Mrenna and P. Skands, *A brief introduction to PYTHIA 8.1*, Comput. Phys. Commun. **178** (2008), 852–867, [[arXiv:0710.3820](#) [hep-ph]].
- [115] D. Amati and G. Veneziano, *Preconfinement as a Property of Perturbative QCD*, Phys.Lett. **B83** (1979), 87.
- [116] A. Bassetto, M. Ciafaloni and G. Marchesini, *Color Singlet Distributions and Mass Damping in Perturbative QCD*, Phys.Lett. **B83** (1979), 207.
- [117] G. C. Fox and S. Wolfram, *A Model for Parton Showers in QCD*, Nucl. Phys. **B168** (1980), 285.
- [118] R. D. Field and S. Wolfram, *A QCD model for  $e^+e^-$  annihilation*, Nucl. Phys. **B213** (1983), 65.
- [119] Y. I. Azimov, Y. L. Dokshitzer, V. A. Khoze and S. Troyan, *Similarity of Parton and Hadron Spectra in QCD Jets*, Z.Phys. **C27** (1985), 65–72.
- [120] Y. I. Azimov, Y. L. Dokshitzer, V. A. Khoze and S. Troyan, *Humpbacked QCD Plateau in Hadron Spectra*, Z.Phys. **C31** (1986), 213.
- [121] B. R. Webber, *A QCD model for jet fragmentation including soft gluon interference*, Nucl. Phys. **B238** (1984), 492.
- [122] J.-C. Winter, F. Krauss and G. Soff, *A modified cluster-hadronisation model*, Eur. Phys. J. **C36** (2004), 381–395, [[hep-ph/0311085](#)].